RESEARCH ARTICLE | FEBRUARY 10 2023

The ocean fine spray

Alfonso M. Gañán-Calvo

Physics of Fluids 35, 023317 (2023)
https://doi.org/10.1063/5.0139151

Physics of Fluids ARTICLE scitation.org/journal/phf

The ocean fine spray

Cite as: Phys. Fluids **35**, 023317 (2023); doi: 10.1063/5.0139151
Submitted: 18 December 2022 · Accepted: 21 January 2023 ·
Published Online: 10 February 2023

Alfonso M. Gañán-Calvo[a)]

AFFILIATIONS

Department Ing. Aerospacial y Mecánica de Fluidos, Universidad de Sevilla, Camino de los Descubrimientos, s/n 41092, Spain and Laboratory of Engineering for Energy and Environmental Sustainability, Universidad de Sevilla, 41092, Spain

[a)]Author to whom correspondence should be addressed: amgc@us.es

ABSTRACT

An important fraction of the atmospheric aerosols comes from the ocean spray originated by the bursting of surface bubbles. A theoretical framework that incorporates the latest knowledge on film and jet droplets from bubble bursting is here proposed, suggesting that the ejected droplet size in the fine and ultrafine (nanometric) spectrum constitutes the ultimate origin of primary and secondary sea aerosols through a diversity of physicochemical routes. In contrast to the latest proposals on the mechanistic origin of that droplet size range, when bubbles of about 10–100 μm burst, they produce an extreme energy focusing and the ejection of a fast liquid spout whose size reaches the free molecular regime of the air. Simulations show that this spout yields a jet of sub-micrometer and nanometric scale droplets whose number and speed can be far beyond any previous estimation, overcoming by orders of magnitude other mechanisms recently proposed. The model proposed can be ultimately reduced to a single controlling parameter to predict the global probability density function of the ocean spray. The model fits remarkably well most published experimental measurements along five orders of magnitude of spray size, from about 5 nm to about 0.5 mm. According to this proposal, the majority of ocean aerosols would have their extremely elusive birth in the collapsing uterus-like shape of small bursting bubbles on the ocean surface.

I. INTRODUCTION

The basic mechanism of fine seawater fragmentation, essential for primary ocean aerosol production, is the bursting of bubbles produced by breaking waves (Fig. 1). From ultrafine to coarse size, the bubble bursting (BB) spray leads to the nascent sea spray aerosols (nascent SSA or nSSA), and primary and secondary marine aerosols (PMA and SMA) whose composition and transport depend on the size of the initial droplets and their bio-physicochemical route along their lifetime.[1–10] These aerosols determine vital self-regulating planetary mechanisms from the water cycle dynamics to the atmospheric optical thickness and planetary albedo via aerosol micro-physics (cloud nucleation, chemical reactions, and catalyzed condensations) with a dominant impact on the radiant properties of atmosphere and global climate, among other primary effects. Current literature[4,6,9–13] report the varying chemical composition of ocean aerosols and their dependence on their size range and the ambient (temperature and wind speed), geographical (latitude and longitude), or lifetime (pH and biological activity) parameters. However, knowing with precision their ultimate origin is often a hopeless task: their generation usually entails extremely elusive phenomena. Indeed, one of the smallest scale, most elusive, extraordinarily fast, yet ubiquitous phenomena of continuous media is the emission of droplets from the bursting of small bubbles at the surface of water.

Incomplete or incorrect causal attributions in science are strongly correlated with the limitations of instruments and tools able to observe the very large or very small spatial and temporal scales,[14] limitations which often lead to periods of stymied progress. However, the assembly of indirect evidence from multiple sources and methods[12,15] is the usual process of advancement. This work presents a thorough revision of the physics of bursting bubbles and their associated statistics and proposes a global statistical model to describe the size distribution of the average ocean spray.

The *average* sea surface is obviously a two-dimensional planar surface (spherical, at planetary scales), as is the surface of still water. Its average radius of curvature is, therefore, nearly infinite (at local scales). However, the open sea surface is a dynamical fractal object whose actual average dimension would astound us. Moving drops, bubbles, liquid ligaments, films, spumes, and dynamic structures of all scales from tens of meters down to nanometers expose a very significant volume of liquid per unit surface to the air and cause the strong mass transfer observed between air and seawater. That volume per unit surface correlates with the local radius of curvature of the dynamical sea surface, which may be from meters to around the millimetric scale at coastal or open ocean turbulent conditions. Just as air is saturated with vapor, long-term turbulent motions keep near-surface seawater layers

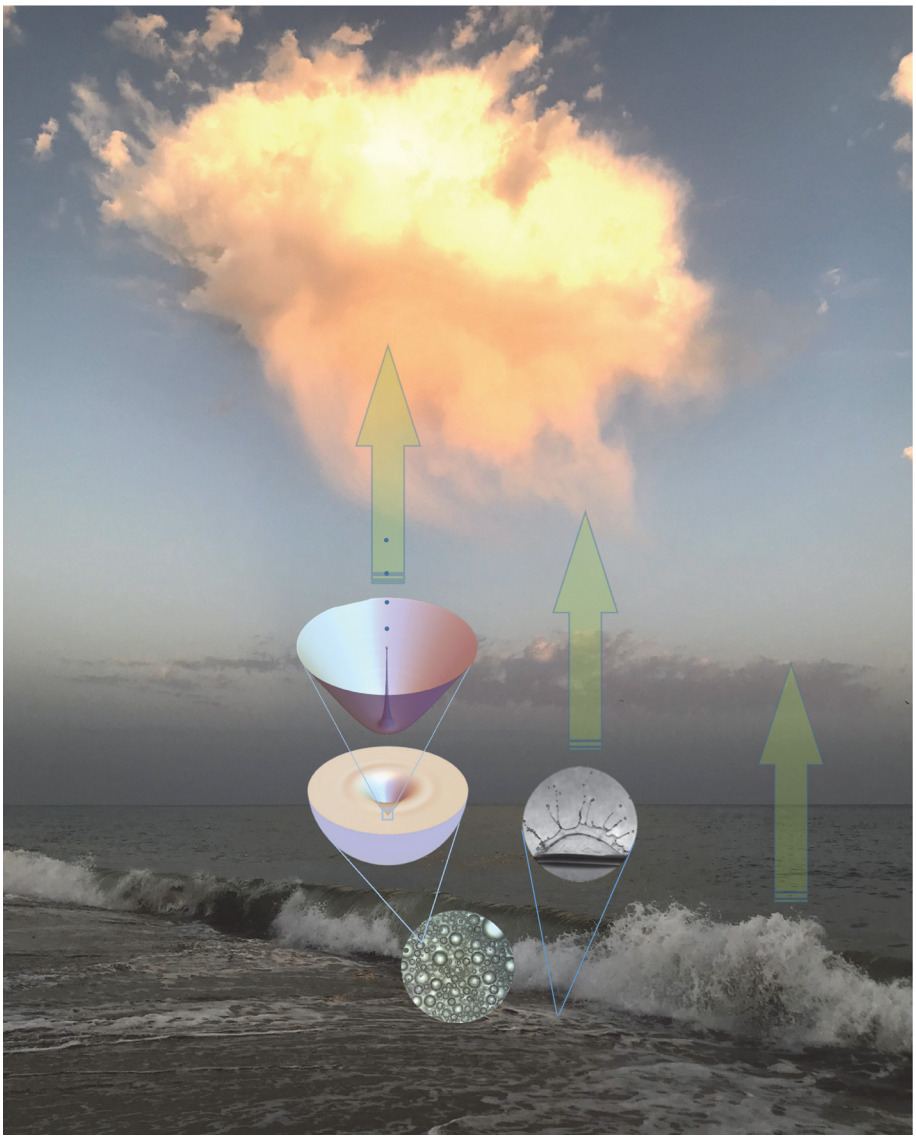

FIG. 1. Marine environment from which a continuous flow of primary aerosols is generated, schematically indicating the basic mechanisms of spray formation: turbulent fragmentation (spume drops) and bubble bursting (film and jet droplets). Jet droplets from microscopic bursting could be not only much more numerous than initially thought but also their extremely small size, in the range of free molecular flow, and their astonishing ejection speed could make them the main source of aerosols in the atmosphere. (Original photograph by the author made at La Antilla, Huelva, Spain, during sunset, pointing Southwest, August 2020. The sun is illuminating the cloud from the right, while the beach is in twilight.)

not only saturated with air but also supersaturated at the air overpressure found inside the smaller, sub-millimetric bubble size range present (in quasi-steady average conditions) in each water layer. Those bubbles become increasingly exposed to the water–air interface as the average value of the surface radius of curvature decreases, and the surface turbulent velocity increases. In fact, they are especially present in surface drops, unsteady films, ligaments, or spumes whose sizes are over one order of magnitude larger than sub-millimeter and micrometer bubbles. Therefore, the surface overexposure to which these small-scale bubbles are subjected causes them to burst at much higher rates than those observed under laboratory or stationary surface conditions. The complexity of open sea conditions is exacerbated by the still unclear aggregated influence of the temperature, presence of particles, and the wind variable.[12,16–20]

Two basic mechanisms are responsible of droplet emission from bubble bursting: bubble film breakup[15,21–26] and jet emission.[21,22,27] Due to their inertia and relatively short settling time, aerosols in the supermicrometer range originating in the ocean would only be measured in marine and coastal regions.[28] In contrast, the sub-micron aerosol size range encompassing the Aitken (10–100 nm) and the accumulation (100 nm to about 1 μm) modes,[29] where cloud condensation nuclei (CCN) and ice nucleation particles (INP) are included, is present everywhere in the atmosphere up to the stratospheric layers.

The origin of the sub-micron aerosol population has been historically attributed to the smallest size range of film breakup droplets,[22,30–32] an idea that has not been challenged until the recent work of Wang *et al.*[12] These authors were probably the first ones quantitatively demonstrating that jet droplets could be more important than previously thought. They imputed the differences found in the

chemical composition of their collected aerosols to the potentially different origin of the liquid coming from either the bubble film or the emitted jet. However, that difference could also be imputed to the changing relative size of the smaller bursting bubbles compared to the surface microlayer thickness.[33] Indeed, bubble sizes below 10 μm at the liquid surface would make the chemical composition of either their jet or film drops indistinguishable since both would drag liquid from the interfacial boundary layer whose average thickness is larger than 10 μm.[34] It is true that when the seawater surface relaxes (corresponding to still conditions), the chemical composition varies in scales as small as some nm from the surface (see Hardy,[34] Fig. 4). However, as their rise time is too large, most of the bubbles of about 10 μm would only come out at the water surface if and only if-they are turbulently drawn and forcedly exposed to the water surface via moving water volumes (subject to external forces) with scales in the millimetric and sub-millimetric ranges. Their surface conditions are obviously far from still and relaxed, and therefore, the chemical separation hypothesis of Wang *et al.*[12] found in laboratory conditions is challenged in open ocean ones.

In a recent work, Berny *et al.*[35] have also pointed to jet droplets as the potential cause of aerosols in the range down to 0.1 μm with maximum number probability density, according to these authors, around 0.5 μm. Indeed, dimensional analysis and up-to-date models reveal that jet drops from bursting seawater bubbles with sizes from about 15 to 40 μm can yield at least tens of sub-micrometer jet droplets with sizes down to about 200 nm.[36–38] Moreover, Berny *et al.*[39] observed the ejection of secondary jet droplets, sensitive to initial conditions of the bursting process, much smaller than the primary ones.

A bold proposal has been very recently published[15] to explain the sub-micrometer SSA origin from film droplets: the film flapping mechanism.[40] This mechanism aims to complement the film bursting described by Lhuissier and Villermaux[26] for the complete description of the spray size distribution, disregarding jet droplets. To the best of our knowledge, Jiang *et al.*[15] and Néel and Deike[41] provide the most comprehensive collection of experimental data on collective bubble bursting so far. In particular, the data of Jiang *et al.*[15] offer a highly valuable statistical disaggregation of the ejected droplet size by both bubble and droplet size variables. In addition, the recent works of Berny *et al.*[35,39] are probably the best sources of numerical information on collective bubble jetting to date. However, the fact that the experimental sub-micrometer measurements of Jiang *et al.*[15] could be contaminated with jetting droplets cannot be ruled out. Indeed, it would be impossible to irrefutably attribute the mechanistic origin of their sub-micrometric measurements to either jet or film drops, as shown in the present work.

Bubble bursting (BB) is a common phenomenon of liquid phase. However, liquids with a low viscosity and relatively large surface tension exhibit special features. Let us consider the average density, viscosity, and surface tension of seawater at the average surface temperature of ocean (15 °C): $\rho = 1026\,\mathrm{kg\ m^{-3}}$, $\mu = 0.001\,22$ Pa s, and $\sigma = 0.0743\ \mathrm{N\ m^{-1}}$, respectively. The best reference measures to describe the physics of BB are the natural scales of distance, velocity, and time defined as $l_\mu = \mu^2/(\rho\sigma) = 19.5$ nm, $v_\mu = \mu/\sigma = 61$ m/s, and $t_\mu = \mu^3/(\rho\sigma^2) = 0.32$ ns for seawater. These scales allow the rationalization and comparison of the different extremely rapid mechanisms of droplet generation. Physical similarity is especially useful for investigating droplet generation from BB, since it is, in principle (assuming negligible dynamical effects of the environment), a conceptually simple biparametric dimensional problem defined by the Laplace and Bond numbers, $\mathrm{La} = R_o/l_\mu$ and $\mathrm{Bo} = (R_o/l_g)^2$, respectively, where $l_g = (\sigma/(\rho g))^{1/2}$. The alternative Ohnesorge number $\mathrm{Oh} = \mathrm{La}^{-1/2}$ is also widely used.

Using all data provided by Berny *et al.*,[35,39] Néel and Deike,[41] and Jiang *et al.*[15] among other valuable information and data resources, jet and film droplet generation from seawater are here exhaustively revised under current available theoretical proposals[15,38] and experimental evidence. Disaggregated data and detailed experimental description in Jiang *et al.*[15] allow reliable statistical resolution of ambiguities in the origin of droplets in the micrometer and sub-micrometer ranges.

In this work, a comprehensive physical rationale for the spray generation from the ocean is proposed, incorporating all possible mechanisms (film bursting, film flapping, and jetting) into a global model. The associated statistics and physical models are reduced to closed mathematical expressions fitted to the existing supporting data. The expressions obtained are subsequently integrated into the general statistical model of the ocean spray proposed. This model predicts the number concentration [probability density function (pdf)] of the average oceanic spray size. The proposed model is compared with an extensive collection of ocean aerosol measurements. To do so, the measured particle size (diameter) is converted to the presumed originating droplet radius, assuming evaporation in the majority of cases, and some degree of condensation for the smallest aerosol size ranges (see Appendix B). The surprising agreement with experimental measurements found along five orders of magnitude of droplet radii r_d would provide a strong confidence on the proposed description: the quantitative agreement suggests that the origin of both primary SSA and SMA would definitely be bubble jetting, with a minor contribution—if any—of film flapping droplets.[15] In this regard, the extremely small length and time scales reached in bubble jetting around bubble collapse lead to local instantaneous rarefied conditions in the gas phase at the collapsing cavity bottom, where Knudsen numbers of the order unity are overcome. This goes in the opposite direction as that demanded by the arguments of Jiang *et al.*, who need sufficiently high gas densities to observe the film flapping mechanism. The latter issue is analyzed in more detail next.

II. DROPLET STATISTICS PER BURSTING EVENT

A. Film droplets: Statistics

The generation of droplets in the micrometer-size and above from the disintegration of the bubble cap film rims is exhaustively described by Lhuissier and Villermaux[26] and references therein. On the other hand, the physics of the film flapping proposal for the production of sub-micrometer droplets by Jiang *et al.*[15] is described in detail in that work. Their experimental results for bubbling in still laboratory seawater and salt water allow a detailed disaggregated statistical analysis of droplet generation (droplet radius scaled as $\chi_d = r_d/l_\mu$) per bubble size, see Fig. 2(a). Interestingly, a very useful scaling law for our purposes can be found from those data. Their experimental probability distributions collapse on a universal lognormal distribution for $r_d \lesssim 0.5\,\mu$m, with a mean value $\langle\chi_d\rangle = \langle r_d\rangle/l_\mu = 1.1\ \mathrm{La}^{1/5}$ and variance $\nu = 0.5$. This data collapse seems to occur for equivalent bubble radii from $R_o \sim 35\mu$m up to 0.7 mm as a function of the Laplace number $\mathrm{La} = R_o/l_\mu$, as shown in Fig. 2(b).

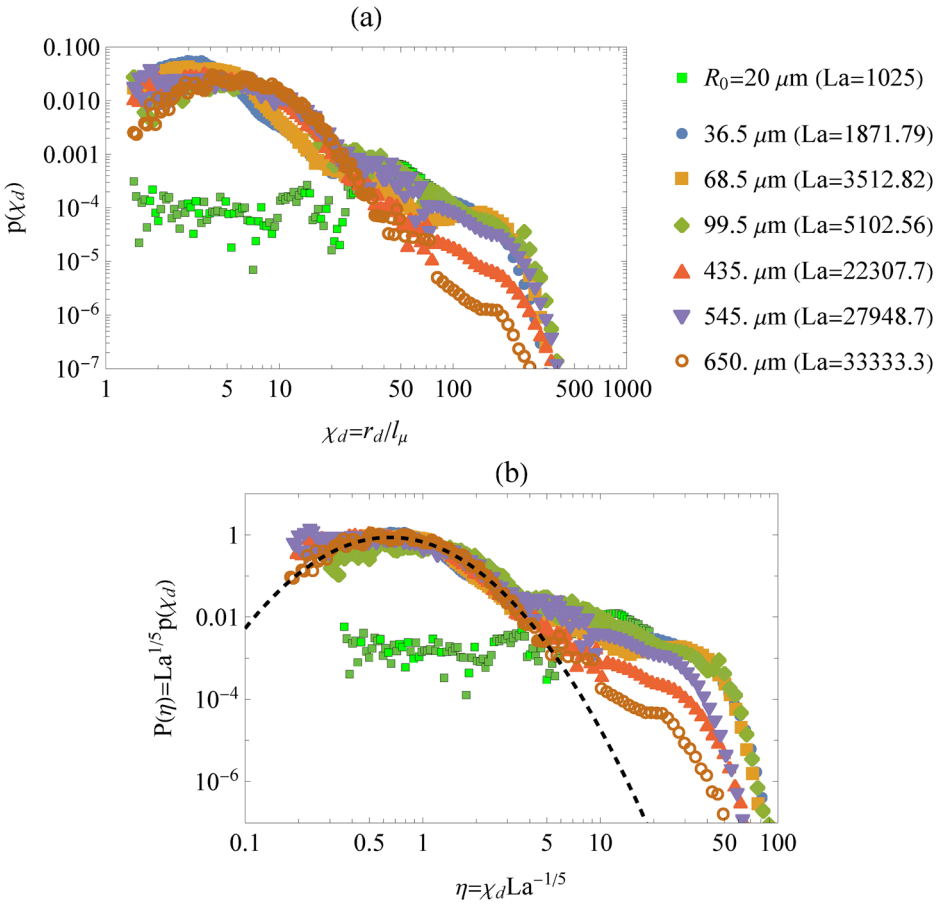

FIG. 2. (a) Probability density function $p(\chi_d)$ as a function of the non-dimensional droplet radius $\chi_d = r_d/l_\mu$. (b) Re-scaled probability distribution $P(\eta) = \text{La}^{1/5} p(\chi_d)$ for the droplet radii scaled as a non-dimensional variable $\eta = \chi_d\ \text{La}^{-1/5}$. For appropriate fitting purposes to a lognormal (thick dashed line), the experimental pdfs[15] are multiplied by 2 to approximately compensate the number contribution for sizes $\eta \gtrsim 4$.

Some caveats must be made about the use of Jiang's laboratory data for modeling:

(a) They use what they call the radius of curvature of the cap as the equivalent bubble radius R_o, which, according to their calculations, is approximately twice the radius of a sphere with the same volume of the bubble for small Bond numbers Bo $= \rho g R_o^2/\sigma$. For bubbles larger than about 0.5 mm, they use Toba's correction.[42] Given that the bubble radius R_o in the literature is that of the equivalent sphere volume,[24,36–38,43] we convert radii to their standard value undoing Toba's correction made by Jiang *et al.*[15] where necessary.

(b) The turbulent ocean surface exposes many orders of magnitude more volume loaded of microbubbles per unit surface than the still surface of a laboratory tank. This fact will produce drastic differences for microbubbles, making any extrapolation from still laboratory tank measurements—at least—doubtful below certain size range.

(c) As Néel and Deike[41] have recently pointed out, there is a very significant difference between the bulk and the surface bubble size distribution that eventually bursts for (i) clean seawater and bubbles around 1 mm and larger and (ii) probably when the residence time at the surface before bursting is long enough to allow accumulation and coalescence.[44]

(d) Despite its crucial interest and potential value, the average bubble size $R_o = 20\mu$m reported in the supplementary information by Jiang *et al.*[15] (La $\simeq$ 1000, coinciding with the critical La$_c$ described in Gañán-Calvo and López-Herrera[38]) has these problems: (i) the surface accumulation and aging could explain the wide distribution of droplet sizes measured, in line with the results of Néel and Deike,[41] and (ii) the reported optical determination of the bubble size in this size range leads to very significant errors. Hence, considering previous observation (b), these measurements will not be used for open sea modeling in the present work.

(e) For La $\sim 10^5$ ($R_0 \sim 2$ mm) and above, a relatively wide range of droplet sizes are produced, as expected from film drops. However, coalescence of bubbles at the water surface and turbulent movements that promote a significant increase in microbubbles that have not been taken into account cannot be ruled out. These latter results are collected and displayed together with the data of Jiang *et al.*[15] for R_o larger than 1 mm in Fig. 3.

(f) The molecular mean free path λ_a in air at atmospheric pressure is about 143 nm. Bubbles with R $<$ 0.2 mm (i.e., $La < 10^4$ for seawater) would produce a film thickness of less than 10 nm ($\ll \lambda_a$). Consequently, an extrapolation of the film flapping mechanism attributed to the film–gas

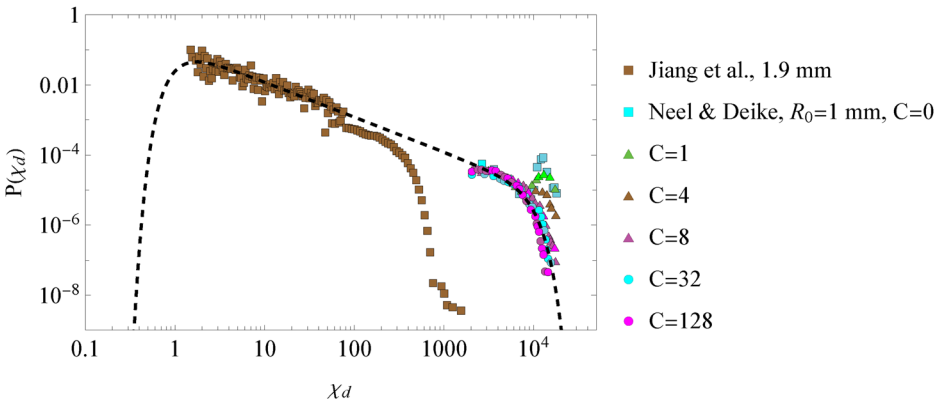

FIG. 3. Probability density function $P(\chi_d)$ for the droplet radii $\chi_d = r_d/l_\mu$ fitted to the experimental data of Jiang *et al.*[15] for $R_o > 1$ mm and of Néel and Deike[41] for different surfactant concentrations. The number densities from Néel and Deike[41] are appropriately scaled to collapse along the ordinates.

interaction at large scales, where the film thickness is comparable or larger than λ_a, would be hardly justifiable.[45]

The experimental setup and measurement equipment used in Jiang *et al.*[15] may not allow precise determination of the numerical concentration of droplets for radii of about ten micrometers or larger due to impact and sedimentation, which would explain the rapid decay of $\chi_d \gtrsim 350$. In contrast, the direct optical measurements of Néel and Deike[41] reliably cover droplet sizes up to 0.4 mm. These latter authors find two types of droplets (see Fig. 3) that can be attributed to film breakup (their collapsing data independent of the surfactant concentration C) or jetting (their peaks around 0.2 mm), which would agree with jet droplet size predictions.[38,39,46] With these considerations in mind, an ensemble pdf can be constructed and fitted to the experimental data after the appropriate scaling of the probabilities reported by Néel and Deike.[41] The data are remarkably well fitted to a generalized inverse Gaussian distribution as

$$P(\chi_d) = \frac{\beta(\langle\chi_d\rangle/\chi_d)^{-1}}{2K_0(\gamma)} \exp\left(-\gamma\left((\langle\chi_d\rangle/\chi_d)^\beta + (\chi_d/\langle\chi_d\rangle)^\beta\right)/2\right), \tag{1}$$

with $\langle\chi_d\rangle = 10^2$, $\gamma = 5\times10^{-5}$, $\beta = 2.4$, and K_0 is the modified Bessel function of the second kind of order 0.

Despite the more than likely mixed contribution of the proposed film flapping mechanism along with classical film bursting and bubble jetting in Jiang's experiments, its value as one of the best sources of data currently available for modeling aerosol generation from bubble bursting roughly in the range of La from about 10^3 to 10^5 is unquestionable. Hence, without challenging Jiang's proposal and observations neither ruling out the potential contribution of alternative mechanisms in their measurements, one may conclude:

(1) The droplet generation in the La range between 10^3 and 10^5, probably due to film flapping, can be assumed to be distributed according to a lognormal for the non-dimensional variable $\eta = \chi_d\ \mathrm{La}^{-1/5}$, which reflects a reasonable dependency on the bubble size, and
(2) For La above 10^5, the more "classical" film rim fragmentation[26] would prevail, yielding droplets distributed according to a generalized inverse Gaussian as (1), independently of La.

B. Jet droplets: Statistics

The phenomenon of bubble jetting can be studied in great detail from both experimental and theoretical approaches.[43,46–48] Figure 4(left) shows three instants of the bursting of a small, nearly spherical bubble at the surface of a liquid: (i) right after the puncture of the thin liquid film, (ii) when the bottom collapses into a nearly conical shape, producing the beginning of ejection, and (iii) when the first droplet is about to be ejected. Consider also the pattern of streamlines at the beginning of ejection (Fig. 4, right, from Gañán-Calvo and López-Herrera[38]) at the bottom of the cavity: this pattern indicates the origin of the liquid ejected as droplets.

Experiments show that there is a critical Laplace number La_c for which the ejected liquid spout reaches a minimum size with maximum ejection speed.[38,43,47,48] For La numbers around $\mathrm{La}_c \simeq 1100$ (see Fig. 4 for La = 918.3 or Oh = 0.033), the influence of density and viscosity ratio with the outer gas environment may become not only noticeable but also crucial to determine these minimum ejected droplet size and maximum speed.[38]

When seawater (and liquid water in general) is involved, though, the phenomenon is not directly observable in the La ranges around La_c due to the smallness of l_μ, and a direct experimental assessment of physical models is not possible. In effect, when gas bubbles from tens to hundreds of micrometers burst at a water free surface, a large numerical fraction of the emitted droplets lies out of the observable range, despite previous efforts by Lee *et al.*,[49] who showed the elusive latest stages of jetting from a 45 μm bursting bubble using x-ray phase-contrast imaging. Even the most precise measuring instruments have limitations concerning the size, speed, or temporal measurability of samples from these ejections. This is because the natural scales of seawater, distance $l_\mu = \mu^2/(\rho\sigma)$ (about 20 nm), and time $t_\mu = \mu^3/(\rho^2\sigma)$ (about 0.32 ns) are involved in the extreme ejection phenomena for bubble radii R_o around $\mathrm{La}_c l_\mu$. These scales are well beyond current optical and imaging instruments. The complexity of the problem is aggravated because those scales are, as subsequently shown, comparable or far below the scales of free molecular flow of the surrounding atmosphere at standard conditions, and hence, the parametric dependency on the density and viscosity ratios with the environment assuming its continuity become meaningless.

Detailed measurements on the first ejected droplet radius R as a function of the normalized bubble radius R_o are available from several authors for an ample collection of experimental and numerical BB

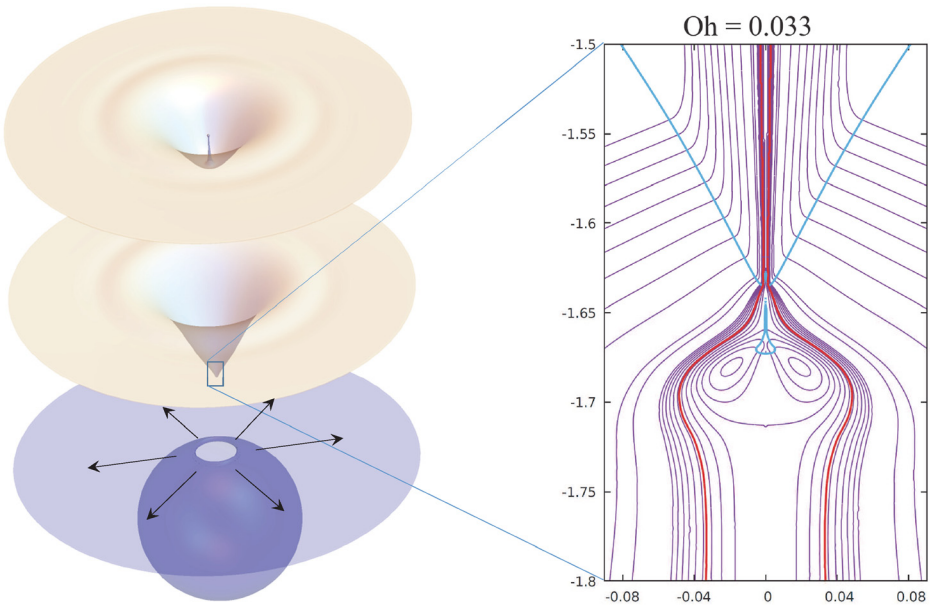

FIG. 4. (Left) Mechanism of bursting from an initially nearly spherical bubble at the surface of a liquid, and (right) streamlines (violet thin lines) of the liquid and air flow around the point of collapse for an instant about $t - t(0) = 10^{-5} t_o$, where $t_o = (\rho R_o^3/\sigma)^{1/2}$, from Gañán-Calvo and López-Herrera.[38] Oh is the Ohnesorge number, related to the Laplace number La $= R_o/l\mu$ as Oh $= \mathrm{La}^{-1/2}$. The blue thick line is the free surface depicted in the left panel. The streamline passing by the point where the vertical velocity of the surface is maximum is highlighted as a thick red curve (see the text).

measurements.[24,36–38,43,48,50–55] The compilation is shown in Fig. 5, where R is scaled with the natural length $l_\mu = \mu^2/(\rho\sigma)$ and is plotted as a function of La. Continuous lines correspond to the theoretical model,[38]

$$R/l_\mu = k_R \mathrm{La}_c \left(\left(\left(\frac{\mathrm{La}}{\mathrm{La}_c} \right)^{1/2} - 1 \right)^2 + \alpha_1 \left(\frac{\mathrm{La}}{\mathrm{La}_c} \right)^{1/2} + \alpha_2 \mathrm{Mo} \frac{\mathrm{La}}{\mathrm{La}_c} \right), \quad (2)$$

with the Morton number $\mathrm{Mo} = \frac{g\mu^4}{\rho\sigma^3} = \mathrm{Bo}\,\mathrm{La}^{-2}$. The best fitting to available experiments yields $k_R = 0.18$, with $\alpha_1 \simeq 0.13$ and $\alpha_2 \simeq 0.19$ (see Gañán-Calvo and López-Herrera,[38] black continuous line).

The different initial conditions of the bursting process and the numerical precision used in simulations may produce a significant variability around the critical La number, $\mathrm{La}_c \simeq 1100$ (corresponding to a critical Ohnesorge number $\mathrm{Oh}_c \simeq 0.03$, see Ref. 38). Interestingly, the data series from each source can be independently and accurately

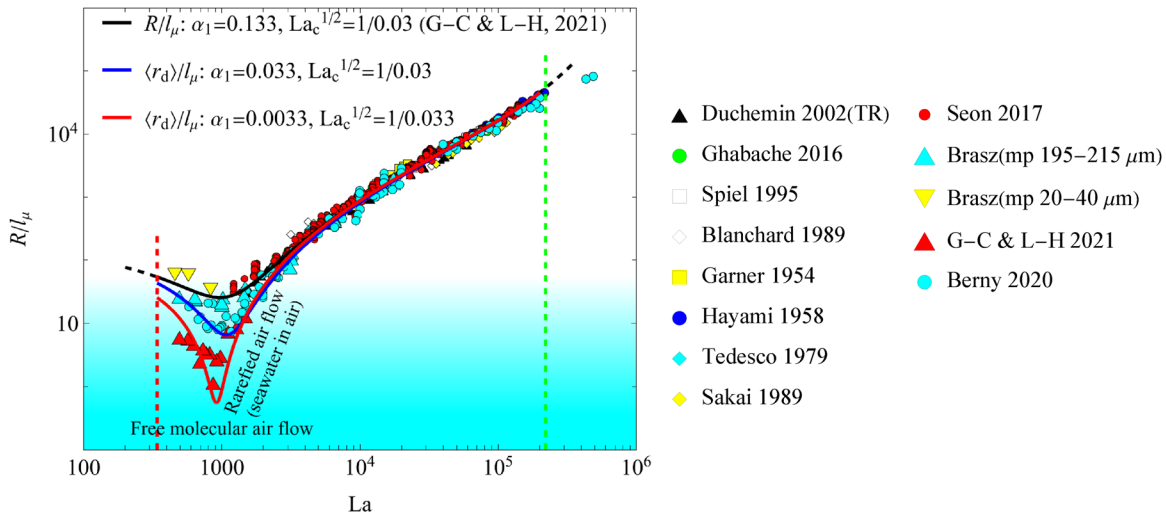

FIG. 5. Radius of the first ejected droplet R as a function of the bubble radius R_o made dimensionless with the viscous-capillary length l_μ, from experimental measurements and numerical simulations taken from the literature (additional information in Ref. 38). The different sets of La_c and α_1 values (continuous lines) fit to different datasets in the range of Laplace numbers La $= R_o/l_\mu$ (abscissae) from the minimum one $\mathrm{La}_{min} \simeq 400$ to about La $\sim 2 \times 10^5$. Bubbles from 8 μm to 2 mm cover the range of La numbers marked by vertical red and green dashed lines for seawater properties at $T = 15\,^\circ$ C. The shaded cyan region indicates the drop size range for air bubbles in seawater for which rarefied conditions are reached: the cyan intensity represents approximately the hyperbolic tangent of the logarithm of the Knudsen number Kn $= \lambda_a/r_d$ [i.e., $1 - 2/(1 + \mathrm{Kn}^{-2})$], where $\lambda_a \simeq 144$ nm is the molecular mean free path of air at average ocean atmospheric conditions.

fitted by different α_1 values, keeping the same k_R and α_2. This fitting parameter α_1, which measures the relative magnitude of the surface tension pressure to produce the initial droplet, compared to the dynamic pressure, plays a determining role when La $\simeq$ La$_c$ [see expression (2)]. Indeed, the crucial importance of α_1 as a measure of the ultimate energy balance taking place at the bubble collapse under critical conditions will be evidenced in Secs. II B 1–II B 3: the smaller the α_1, the larger the mechanical energy per unit volume available at the focus point of collapse in the initial instants of ejection, and the larger the number of droplets with scales at or below l_μ that could be generated. Also, the data in Fig. 5 correspond to the radius of the first ejected droplet, R.

However, the emission lasts during times comparable to, or longer than the capillary time $t_o = (\rho R_o^3/\sigma)^{1/2}$, much larger than the time of formation of the first droplet at the front of the issuing liquid ligament $t_c = (\rho R^3/\sigma)^{1/2}$ since $R \ll R_o$. Thus, the high-speed liquid ligament has long time to elongate and disintegrate into a large number of droplets with a variety of radii r_d.[39] In these conditions, the density and viscosity of the outer medium can dramatically alter the breakup of the spout into droplets.

1. High-speed nanometric jet breakup in a rarefied environment

The impact of the environment rarefication was demonstrated reducing the viscosity and density of the outer environment one order of magnitude, which keeps the high velocity of the jet front for a longer time. Indeed, the bubble radius corresponding to La$_c$ (minimum r_d) is $R_o \simeq 20\,\mu$m. This would lead to drop radii well below the mean free path of gas molecules of the environment ($\lambda_a \simeq 143.5$ nm in air at average ocean atmospheric conditions), and ejection speeds above their average molecular speed (around 485 m/s in standard conditions). Hence, the values of the fitting constant α_1 should reflect the very different ratios of initial surface tension to dynamic pressures as the Knudsen number Kn $= \lambda_a/r_d$ varies among liquids[48,55] under laboratory conditions.

A brief inspection of the values attained for the sizes and speeds of these droplets around a critical value La$_c \simeq 1100$ (e.g., Refs. 37, 38, and 55) for seawater shows that they are, indeed, in the range of ultrafine aerosols, with sizes well below the molecular mean free path (around 70 nm in air at standard conditions) and velocities exceeding by far the average molecular speed of the surrounding gas (around

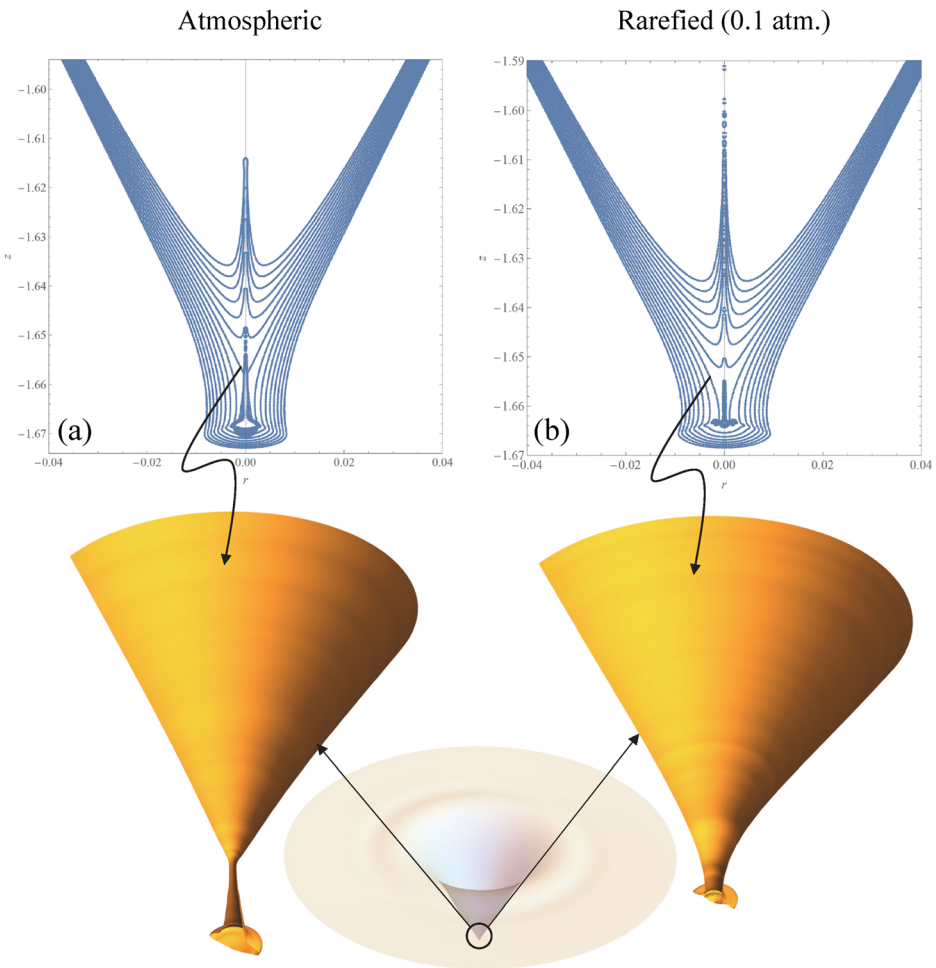

FIG. 6. The shape of the axisymmetric collapsing free surface at the bottom of the bursting bubble, at 15 successive instants around the time of collapse t_o with constant time intervals $\Delta t = 10^{-5} t_c = 1.9245 \times 10^{-3} t_\mu$, for Oh = 0.03. Density and viscosity ratios are $\varphi = \rho_g/\rho = 0.001$ and $\eta = \mu_g/\mu = 0.01$, respectively, and (b) $\varphi = 0.0001$, $\eta = 0.001$ (rarefied gas conditions, 0.1 atmospheres). Numerical simulations from Gañán-Calvo and López-Herrera[38] made with Basilisk[56] using level 15 (simulations made by López-Herrera). Observe the shape of the collapse neck: while the minimum radius is located at a certain distance from the bottom of the cavity for standard gas densities (in the continuum hypothesis), it is nearly at that bottom in the rarefied conditions.

290 m/s). In these extreme cases, the consideration of a stochastic, extremely rarefied environment would be the most realistic assumption. No one has ever simulated this complex phenomenon, let alone directly observed it, completely beyond the capabilities of current measurement techniques, and its direct visualization or assessment is impossible.

The evolution of high-speed nanometric jets in vacuum using molecular simulations has been reported in the literature.[57] These simulations show the rapid action of surface tension, even under a non-continuous approach, in terms of equivalent local Weber and Ohnesorge numbers $\mathrm{We} = \rho v^2 d_j/\sigma$ and $\mathrm{Oh} = \mu/(\rho\sigma d_j)^{1/2}$, respectively, where d_j (much smaller than l_μ) is the local diameter of the liquid ligament. To achieve a high ejection velocity bypassing the action of viscous forces at these extremely small scales, a huge energy density much larger than $\mu^2/(\rho d_j^2)$ should be locally applied (Fig. 6). For seawater and d_j around 5 nm, the energy density involved should be greater than about 5×10^7 Pa.

In this regard, we observe that the collapse of the neck occurs much closer to the bottom (i.e., the gas volume of the trapped bubble is significantly reduced) under rarefied conditions, which produces an enhanced kinetic energy focusing at the instant of collapse and a significant excess of ejection velocity compared to the speed of sound at atmospheric conditions. This is a key consideration that also applies to other similar jetting processes like flow focusing or electrospray[58] that can lead to the formation of nanometer-sized droplets.[59] Once the jet is ballistically ejected, the local action of surface tension immediately promotes the fragmentation of the ligament and the production of droplets[60] if the dynamical effect of the environment is negligible (e.g., rarefied gas or vacuum).

In contrast, the numerical simulations of BB made so far[37,38,43] assume the continuum hypothesis,[56] which excludes the possibility of a rarefied or vacuum environment and the early action of surface tension observed in real conditions. However, even under continuum assumptions, a reduction of the outer density fosters the early spout breakup, too. An illustration of the onset of an extreme emission event (very small sizes and large ejection velocities) with a reduced density and viscosity gas–liquid ratios ($\varphi = \rho_g/\rho$ and $\eta = \mu_g/\mu$, respectively) is given in Fig. 7. It shows a sequence of up to six extremely small initial droplets ejected consistently with previous statistical analysis[35,60] if the number of ejected droplets n_d is sufficiently large. Indeed, from the values of the two subsequent times here considered, the initial frequency of droplet ejection is extremely high, about $4 \times 10^5\, t_o^{-1}$. In addition, in Gañán-Calvo and López-Herrera,[38] we report the ejection of droplets as small as two times the viscous-capillary length l_μ for La = 1000 using numerical simulation. This corresponds to droplets with radii of 40 nm, or to 10 nm dry particle radius using seawater.

I propose that the ejected droplets can reach radii as small as 4 nm and below at the bottom of the cavity collapse corresponding to La = 1000 using seawater with air at atmospheric conditions. This is possible because these atmospheric conditions can statistically allow instantaneous vacuum conditions, for the extremely short final collapsing times: the local length scales yield Kn values above 1 since the front radius of curvature of the ejected spout can reach sizes below 0.2 times l_μ (Fig. 2 in Gañán-Calvo and López-Herrera[38]). The smallest experimentally reported particle radii are about 1.5 nm,[61,62] corresponding to about 6 nm droplet radii. Based on these arguments, although obtaining direct evidence for the origin of these particles is impossible, the bubble jetting phenomenon is a well-justified candidate for primary SSA and pristine ocean aerosols in this range.

Thus, the central spout ejected by small collapsing bubbles in seawater could yield much more numerous droplets, their size could be much smaller, and their ballistic speed much larger than previously expected. Numerical simulations show[38] that their size, production frequency, and speed can reach values well beyond the natural scales of seawater at the average temperature of the ocean (15 °C), i.e., $l_\mu = 19.5$ nm, $t_\mu^{-1} = 3.11 \times 10^9 \mathrm{s}^{-1}$ ns, and $v_\mu = 61$ m/s, respectively. The size, frequency, and velocity of the ejected droplets in simulations can be, respectively, 10–20 nm (depending on temperature and

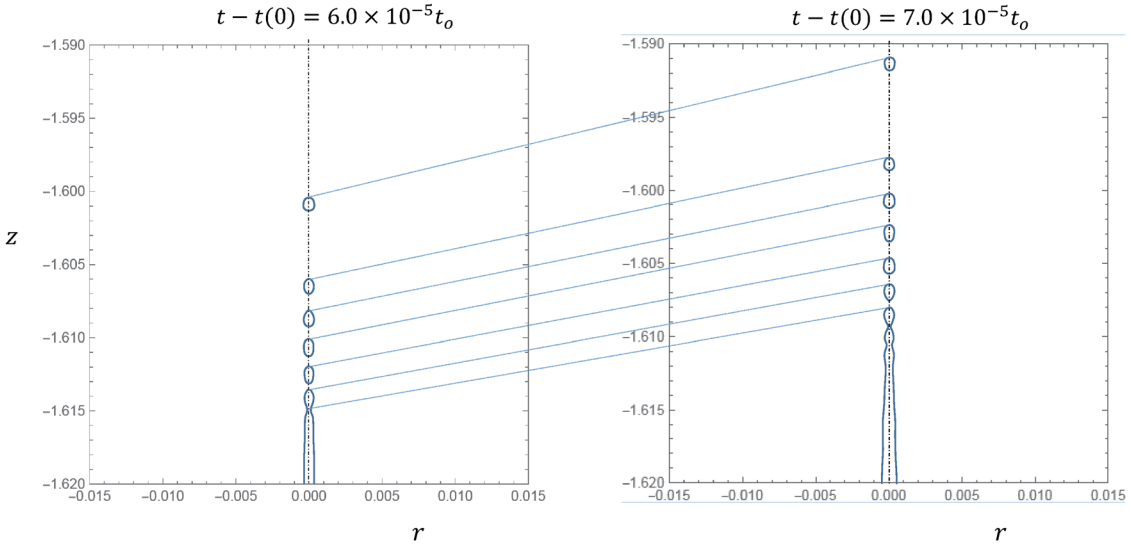

FIG. 7. Two successive instants of the ballistic ejection of the first six droplets for La = 1111 (Oh = 0.03) in rarefied conditions ($\varphi = 0.0001$, $\eta = 0.001$) at average sea level and temperature[38] (simulations made by López-Herrera). The resulting radii are about 7.5 nm for seawater.

salinity), around the GHz frequency, and 300–600 m/s (Ref. 38, i.e., beyond the thermal speed of molecules of the surrounding gas air). Consequently, they can reach distances well beyond any previous considerations.

Although a systematic analysis and direct quantification of the rarefaction effect proposed here do not yet exist due to its extraordinary difficulty and elusive nature, the evidence described here is sufficient to consider it of interest. In particular, this work proposes a global framework in which the number of droplets generated can be quantitatively linked by a single parameter to that precise physical feature (rarefaction effect) in the bubble breakup process. If such a framework shows the ability to reproduce the global characteristics of the measured aerosols, it would definitely merit consideration. That framework and its capability are described in detail and challenged throughout Secs. II B 2 and II B 3.

2. Earlier evidences of the role of ultrafine jet drops

Regarding the chemical composition of the measured spray, Wang *et al.*[12] made a fundamental insight to determine differences that could be ultimately assigned to either film or jet drops. In fact, the film droplets are richer in species of the molecular layers closer to the surface. In contrast, despite the presence of a recirculating region (see Fig. 4), the streamline pattern indicates that the material ejected as jet droplets should be a sample from the liquid bulk,[38] not the surface, consistently with the results from Wang *et al.*[12] The results of Wang *et al.* raised a crucial issue in the field. However, as the bubble size decreases down to the micrometric scale, the liquid sample in the droplets should be increasingly dominated by the sea surface microlayer composition,[33] even for jet droplets. In addition, given the extremely small size of the liquid relics, their acidity and consequent reactivity could reach high levels,[9] together with their capability to immediately nucleate or react with volatile organic components (VOC) present in the surrounding atmosphere.[6] Thus, below certain sub-micrometer droplet size, to observe distinctions of kinematic origin from the physicochemical nature of the eventual seawater aerosol becomes impossible with current equipment and experimental setups. Nonetheless, the findings by Wang *et al.*,[12] the analyses of Berny *et al.*[35,37] and Berny *et al.*,[39] and previous considerations would point to the jet droplets as a potential origin of at least a major fraction of sub-micrometer SSA and SMA present in the atmosphere.

Interestingly, Wang *et al.*[12] specified $R_o = 13$ and $4\,\mu$m as the bubble size responsible of the highest measured sound frequency from breaking waves[63,64] and the minimum bubble size capable of producing jet drops,[49] respectively, without resorting to any physical description of the bubble breakup mechanism. In reality, the two bubble sizes $R_o = 13$ and $4\,\mu$m aforementioned approximately correspond to the two key values of the Laplace numbers $\mathrm{La}_c = 1111$ and $\mathrm{La}_{min} = 343$, respectively, reported in the literature (i.e., $\mathrm{Oh}_c = 0.03$ and $\mathrm{Oh}_{max} = 0.054$, respectively,[37,38,43,46–48,55]). These Laplace numbers correspond to:

(i) The minimum radius of the first ejected droplet for the whole spectrum of jet emitting bubbles, and
(ii) The minimum bubble radius $R_{o,min}$ for which jet droplets are ejected.

3. The probability density function of jet droplet size

Given the difficulty of direct measurements of jet droplet statistics, researchers have relied on numerical simulation. Deike and coauthors[35,39] studied the variability of data sizes along the whole transient jet emission event, an essential ingredient of any statistical global model. These authors offer a very ample set of data under "noisy initial conditions" for all-drops ejected droplet radii r_d from simulations, with La numbers spanning close to three orders of magnitude. A best fitting statistics of these data to a Gamma distribution,[60]

$$p(\chi_{d,i}) = \frac{\alpha^\alpha}{\Gamma(\alpha)} \chi_{d,i}^{\alpha-1} \exp\left(-\alpha\chi_{d,i}\right), \tag{3}$$

yields a shape factor α dependent with La approximately as $\alpha = 0.65\,\mathrm{La}^{1/5}$. Here, $\chi_{d,i} = r_{d,i}/\langle r_d\rangle$, and r_d is, for each bursting event, a statistical variable where its average $\langle r_d\rangle$ is a function of La with the same form as (2) but a different α_1 value (i.e., a different ratio of surface tension to kinetic energy at the front of the spout) than the one of the first droplet R: in general, $R \neq \langle r_d\rangle$. Note the appearance of the power 1/5 affecting La in the jet droplet like in the film flapping droplets statistics, whose analysis is beyond present study.

The fitting used a modified Anderson–Darling test as follows. The data are represented in Fig. 8 as the cumulative distribution value F_i for each i-droplet of radius $r_{d,i}$ divided by $(1 - F_i)$ vs the theoretical values corresponding to a Gamma distribution, i.e., $\Gamma_{R,\alpha}(\chi_{d,i})/(1 - \Gamma_{R,\alpha}(\chi_{d,i}))$, where $\Gamma_{R,\alpha}(\chi_d) = \Gamma(\alpha, 0, \alpha\chi_d)/\Gamma(\alpha)$ is the normalized cumulative Gamma distribution function. We observe a reasonable global statistical goodness-of-fit for the whole range of La numbers explored (about three orders of magnitude). This guarantees a sufficient confidence on the assumption that the breakup of the time-evolving ejected liquid ligament approximately follows a Gamma distribution as predicted by Ref. 60, with a La-dependent shape factor $\alpha = 0.65\,\mathrm{La}^{1/5}$.

C. The number of ejected droplets per bursting event

1. Film drops

Jiang *et al.*[15] give very useful experimental values of the number of droplets ejected per bursting event in their Figs. 3(b) and S6. Their collection of data from other authors is especially useful too. These data are gathered in Fig. 9, where the two mechanisms, film bursting and flapping, are separately considered according to their characteristic number production.

A particularly notable finding of Jiang *et al.*[15] is their explanation of the Blanchard–Syzdek paradox[23] around $\mathrm{La}_{BS} \simeq 7 \times 10^4$ for seawater ($R_o \simeq 1.4$ for $T = 15\,^\circ$C to 2.3 mm for $T = 5\,^\circ$C), where the film flapping mechanism dominates for $\mathrm{La} < \mathrm{La}_{BS}$, while the film bursting does so for $\mathrm{La} > \mathrm{La}_{BS}$. Since Jiang *et al.* consider R_o as twice that of the equivalent spherical volume radius, their own data do not appear to collapse well with those of the other authors. However, taking R_o as the equivalent spherical radius assumed by the other authors, the collapse of Jiang's data with the rest of authors is evident.

Despite one observes certain degree of overlapping between the film breakup mechanisms due to the complexity of the collective bursting process and its critical dependency on different factors (temperature, pH, presence of surfactants, particles, and organic compounds), there is a relatively clear statistical separation between them.

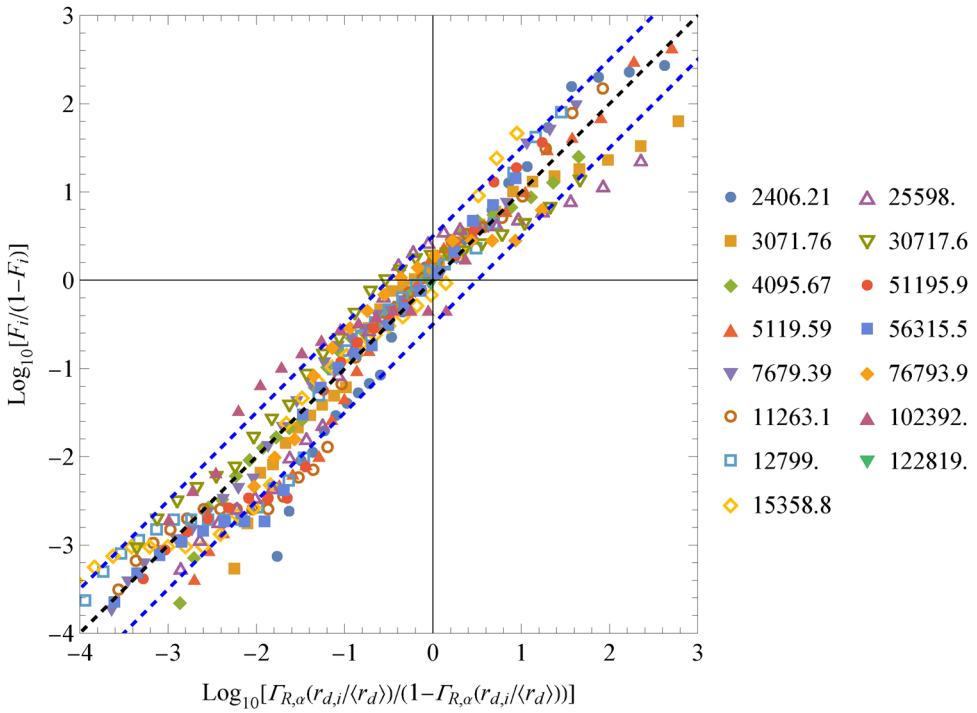

FIG. 8. Statistical test of data from Berny *et al.*[35] against a Gamma function. The test follows a modified Anderson–Darling approach, see text. The right labels are the La numbers of each data series. The blue dashed lines indicate a ± 0.5 deviation.

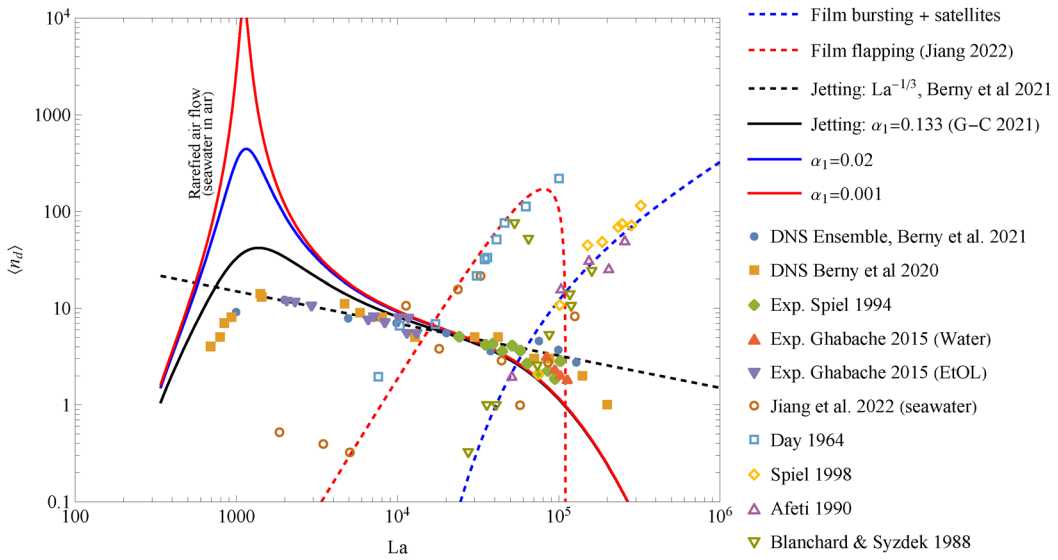

FIG. 9. The average number of droplets ejected per bursting event, $\langle n_d\rangle$. Data gathered from Ref. 35. The continuous lines correspond to the theoretical model (8), for different α_1 values and Mo calculated for seawater at 15 °C. Observe that the size range of bubbles effectively shooting jet droplets is from about 6 to 7 μm (La $\simeq$ 350) to about 2 mm (La $\simeq 10^5$). A direct measurement, visualization, or simulation of ejections for seawater around La_c is impossible: only an indirect assessment is viable.

For the purposes of global modeling, one could separately fit the number of droplets produced by each mechanism by the expressions

$$n_{d,B} = N_B \frac{\mathrm{La}}{\varpi \mathrm{La}_{BS}} \exp\left(-\frac{\varpi \mathrm{La}_{BS}}{\mathrm{La}}\right) \tag{4}$$

for the film bursting droplets, with $N_B \simeq 40$, and

$$n_{d,F} = N_F \left(\frac{\mathrm{La}}{\mathrm{La}_{BS}}\right)^{\alpha_F} \left(1 - \frac{\mathrm{La}}{\mathrm{La}_{BS}}\right), \quad (\text{valid for } \mathrm{La} < \mathrm{La}_{BS}) \tag{5}$$

for the film flapping droplets, with $N_F \simeq 600$ and $\alpha_F \simeq 2.75$. The overlapping is reflected by the factor $\varpi \simeq 1.57$ affecting the value of La_{BS} in (4). These fittings are plotted in Fig. 9.

The number of film bursting droplets tends to scale with La for $\mathrm{La} \to \infty$ since their number would be proportional to the radius of the equivalent volume sphere due to mass conservation: the fragmenting film rim has a length commensurate with the bubble radius, while the film thickness becomes nearly independent of La. However, the marginal dependence of the film flapping droplet number $n_{d,F}$ for decreasing La with the power α_F, between the bubble surface ($\alpha_F \sim 2$) and volume ($\alpha_F \sim 3$), could be related to the decreasing effect of the gas in the bubble and its surroundings by rarefaction (i.e., when Kn increases) as the bubble size and, consequently, the sub-micrometer droplet sizes decrease. The fundamental effect of the bubble gas is well documented by Jiang *et al.*[15] On the other hand, flapping droplets seem to cease abruptly at the Blanchard–Syzdek transition value La_{BS}.

2. Jet drops

The number of ejected droplets is one of the main claims of this work: for seawater, this number can be orders of magnitude larger than any previous estimation based on experiments with other liquids in air or numerical simulation assuming a continuum gas atmosphere. In the bubble size range from about 10 to 100 μm, seawater produces ejections with associated Knudsen numbers above unity and velocities beyond the thermal speed of air. These two facts would lead to much larger droplet fragmentation frequencies (and total ejected droplet number) than previously thought.

The main cause of the extremely large velocity of the issued liquid spout is the radial collapse of an axisymmetric capillary wave at the axis,[38,47,65] producing a singularity[66] and the trapping of a tiny bubble at the bottom of the cavity (see Fig. 6, and Fig. 5 in Ref. 38). The radial collapse elicits a subsequent ejection in the axial direction of an initially quasi-infinitesimal spout of liquid at an extremely large velocity: we observe that the initial droplet ejection velocity in Fig. 7 above can be about $10^3 \times V_o$, where $V_o = (\sigma/(\rho R_o))^{1/2}$ is the characteristic velocity of the bursting process driven by capillary forces.

The ejection velocity of the first droplet V has been investigated in Refs. 37, 38, 43, 46, 48, 55, and 65, among other works. Fitting the speed of emission is trickier than the droplet size, given the dependency of the former on the point at which it is measured and the inherent variability of the liquid spout velocity. If that point is set approximately at the point where the droplet is released, the recent model proposed by Ref. 38 yields

$$V/v_\mu = k_V \left(\left(\left(\frac{\mathrm{La}}{\mathrm{La}_c}\right)^{1/2} - 1 \right)^2 + \alpha_1 \left(\frac{\mathrm{La}}{\mathrm{La}_c}\right)^{1/2} + \alpha_2 \mathrm{Mo} \frac{\mathrm{La}}{\mathrm{La}_c} \right)^{-1/2}. \tag{6}$$

This model is compared with the experimentally measured V in Fig. 10. In general, the scale of the ejection velocity $v(t)$ co-evolves with the radial scale of the ejection $r(t)$ as $r(t) \sim v(t)^{-2}$ along the process (see Ref. 38). This trend is consistent with the valuable data provided by Berny *et al.*[37] for the five first ejected droplets (see Figs. 6 and 7 in Ref. 37). However, while the prefactor k_R is a constant, the best fitting to the experimentally measured and reported V demands that k_V (of order unity) should be slightly dependent on La (Oh) and Bo as $k_V = 0.39 f_v(\mathrm{La,Bo})$. The fitting function f_v proposed by Ref. 38 was $f_v = (1 + k_1 \mathrm{Bo} + k_2 \mathrm{Oh})^{-1}$ with $k_1 = 2.27$ and $k_2 = -16$. A better fitting is here obtained with $f_v = (1 + k_1 \mathrm{Bo} - \mathrm{La}^{\gamma_1})^{-1}(1 - (\mathrm{La}_{min}/\mathrm{La})^{\gamma_2})$, with $\gamma_1 = -0.125$ and $\gamma_2 = 0.8$.

The extremely large initial velocity of the incipient spout rapidly decays as the mean radius of the ejected spout increases along the ejection process. According to high precision numerical simulations[38,67] assuming seawater and air at atmospheric conditions, it decays about

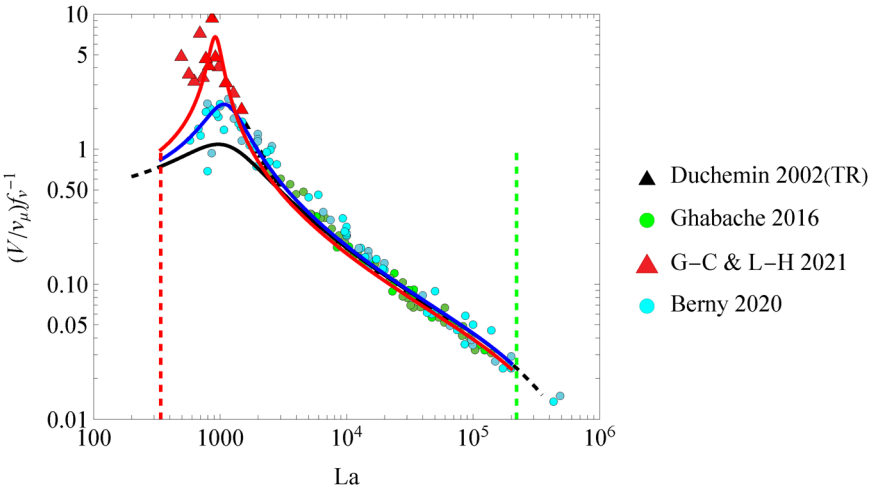

FIG. 10. The measured ejection velocity V of the first drop, corrected with the factor f_v and compared with the proposed model. The curves correspond to the velocity of the first droplet (black line), as fitted in Ref. 38, and the alternative fitting here proposed for the average $\langle v_d \rangle$ (blue line).

an order of magnitude before the first drop is released. Interestingly, the speed of the first droplet V is comparable to or larger than the capillary-viscous or natural velocity $v_\mu = \sigma/\mu$ for La in the range from $La_{min} \simeq 400$ to about 4×10^3 (see Fig. 10), the range where the maximum ejection velocities and minimum jet droplet radius are reached, where the bottom microbubble trapping is prevalent.

For the critical $La_c = 1100$ values where V peaks (where f_v is about 0.52), V can reach values as high as one order of magnitude above v_μ.[38] In contrast to the rest of the domain, which shows robustness to initial perturbations,[39] the parametrical region around La_c is highly sensitive to effects like the gas conditions, as previously explained. In Ref. 38 (see Fig. 2 in that work), we showed that the transversal size of the ejected spout is inversely proportional to its velocity for times smaller than the natural one t_μ from the instant of collapse. Hence, the sooner the ballistic jet starts ejecting droplets, the smaller, faster, and more numerous those droplets will be. In that initial time interval, the velocity of ejection in the simulations (assuming incompressibility) can be as high as 20 times the natural velocity v_μ (about 61 m/s for seawater), with spout sizes about 0.1–0.2 times $l_\mu \simeq 19.5$ nm. In the absence of interactions with the environment, or in conditions of minimized interactions, that initial velocity can overcome the speed of sound in sea air, and—consistently—the emitted droplets can be orders of magnitude smaller than the molecular mean free path of air in standard conditions.

According to Ref. 68 and in the absence of any interaction with the environment, the most unstable wavelength λ for a viscous liquid column of radius r_j is equal to $\lambda = 2\pi\psi r_j/k$, with $k \simeq 0.697$ and ψ a function of $Oh_j = \mu/(\rho\sigma r_j)^{1/2}$ very approximately equal to $\psi = (1 + 2Oh_j)^{1/2}$. Given that the environment surrounding the ejected ligament is a high-speed gas jet (see Fig. 4) co-flowing alongside with that, one can assume that the liquid is moving with a comparable velocity to that of the environment, and its dynamical effect can be, in first approximation, neglected. Thus, the conservation of mass on breakup leads to

$$r_d/r_j \equiv \zeta = \left(\frac{3\pi}{2 \times 0.697}\right)^{1/3} \left(1 + 2(\zeta/\chi_d)^{1/2}\right)^{1/6}, \tag{7}$$

where $\chi_d = r_d/l_\mu$. This is a transcendental function for ζ whose solution can be very approximately resolved for a given χ_d using the fixed point method with initial value $\zeta = 1$ in the right hand side of (7). A couple of iterations (that can be explicitly expressed) yield the solution with maximum errors below 0.1%. The relationship (7) is expected to hold even close to the molecular scale, as demonstrated by Moseler and Landman[57] and Zhao, Lockerby, and Sprittles[69] via molecular simulations of nanojets.

Next, the instantaneous ejection flow rate is proportional to $v_d r_j^2$. Obviously, there is an inherent variability of the ejected droplet radius and velocity along a single bursting, implying the consideration of the two stochastic variables r_d and v_d in the calculations. However, one has that:

(1) There is a strict limitation for the time along which the ejection is active, given by $t_o = (\rho R_o^3/\sigma)^{1/2}$,
(2) As previously seen, both stochastic variables χ_d and $\upsilon_d = v/v_\mu$ have well defined statistics in a single bursting event, with average $\langle\chi_d\rangle$ and $\langle\upsilon_d\rangle$ depending on La and Mo only. These average values should be (universally) proportional to both R/l_μ and V/v_μ in a single bursting event.

Thus, the conservation of total mass along a single ejection event within a continuous bursting of bubbles of different sizes demands

$$n_d \sim t_o \frac{v_d}{r_d}\left(\frac{r_j}{r_d}\right)^2 \sim t_o \frac{\langle v_d\rangle}{\langle r_d\rangle}\zeta^2 \Rightarrow n_d = k_c \mathrm{La}^{3/2}\frac{\langle\upsilon_d\rangle}{\langle\chi_d\rangle}\zeta^2, \tag{8}$$

where both $\langle\chi_d\rangle$ and $\langle\upsilon_d\rangle$ are given by the expressions (2) and (6), with fitting constants $k_{R,V}$ and α_1 that can be different from the original ones for R and V, summarized by the constant k_c. This is justified since (i) α_1 measures the relative weight of surface tension energy to form the droplet at the front of the issuing liquid spout,[38] which can vary along the bursting event, and (ii) the prefactors $k_{R,V}$ should obviously reflect the overall change of both r_d and v_d along the bursting, too.

Hence, one can calculate the single-event averaged number of ejected droplets using (8) as a function of La and Mo alone. Recently, Berny *et al.*[35] sought for a scaling law as $\langle n_d\rangle \sim \mathrm{La}^{-1/3}$. They directly measured the size of ejected droplets using numerical simulations with fixed density and viscosity ratios with the environment. However, our simulations point to the appearance of an enormously larger number of ejected droplets as one decreases those ratios (see Fig. 7) or at those small scales where the gas environment becomes rarefied (close or beyond the molecular mean free path scale), which may apply to the case of water in air for La around La_c.

Indeed, we observe that the fitting constant α_1 in (2) and (6) strongly determines both the minimum droplet radius and the maximum ejection speed for the whole La-span and, therefore, determines the total number of droplets ejected, as shown in Fig. 9.

Fitting the number of droplets ejected per bursting event n_d for seawater to the dataset gathered by Berny *et al.*[35] for La $>10^4$ approximately yields $k_c = 1$. However, the average number of droplets generated could deviate very significantly from Berny's assumption (i.e., $n_d \sim \mathrm{La}^{-1/3}$) for La $<10^4$ assuming rarefied gas conditions, which entails using different α_1 values. The new approach correctly predicts no ejection (i.e., $\langle n_d\rangle \to 0$) as La approaches the two extreme values already mentioned in the literature.[35,37]

D. The bubble statistics

There is an ample literature on the subject of bubble generation in the ocean and its qualitative analysis (e.g., Refs. 16, 22, 63, 70, and 71). The data from Deane and Stokes[16] and Blenkinsopp and Chaplin[70] have been established as a reliable source of experimental measurements of bubble plumes and swarms produced by breaking waves. Figure 11 plots both datasets, where both the sub- ($\sim x^{-3/2}$) and super-Hinze ($\sim x^{-10/3}$) scales[16] are clearly visible. The bubble radius R_o is made dimensionless with the average bubble radius $\langle R_o\rangle$ obtained from the best fitting continuous probability distribution to the datasets from Deane and Stokes[16] and Blenkinsopp and Chaplin,[70] which yields $\langle R_o\rangle \simeq 0.25$ mm. From the fundamental theoretical considerations on the bubble dynamics made by Clarke *et al.*[17] and Quinn *et al.*[20] showing the existence of two clearly defined power-law ranges and a drastic decay below a certain R_o, the use of an analytic extended Singh–Maddala probability density distribution (p.d.f.) $q(x)$ is proposed in this work as follows:

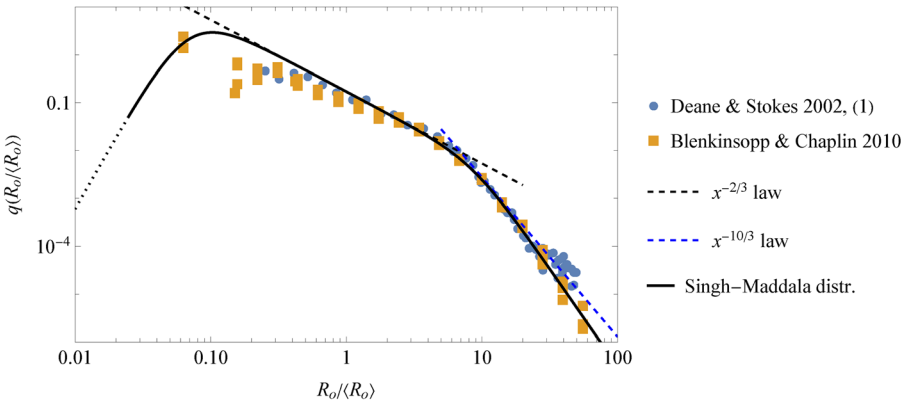

FIG. 11. Probability distribution of the bubble radius R_o produced by breaking waves, made dimensionless with the average bubble radius $\langle R_o\rangle$ of the best fitting continuous probability distribution to the datasets from Deane and Stokes[16] and Blenkinsopp and Chaplin[70] (see the text).

$$q(x) = A\,a\,x^{a-1}\left(1+\left(\frac{x}{\varepsilon X}\right)^{d}\right)^{\frac{1-a+b}{d}}\left(1+\left(\frac{x}{X}\right)^{d}\right)^{\frac{-b+c}{d}} \tag{9}$$

with $b = -3/2$.[17,20] Constants A and X can be analytically obtained from the condition that the s-moments distribution, given by,

$$F(x,s) = A\,x^{a+s}\,{}_2F_1\left(\frac{a+s}{d},\frac{b-c}{d},\frac{-1+a-b}{d},\frac{a+d+s}{d},\right.$$
$$\left.-\left(\frac{x}{X}\right)^{d},-\left(\frac{x}{\varepsilon X}\right)^{d}\right) \tag{10}$$

are equal to 1 for both $s=0$ and 1, i.e., making $F(x\to\infty, s=0) = F(x\to\infty, s=1) = 1$. F_1 stands for the first of the Appell hypergeometric series. Moreover, $x = R_o/\langle R_o\rangle =$ La $l_\mu/\langle R_o\rangle$, $X = \mathrm{La}_{Hinze} l_\mu/\langle R_o\rangle$, and $\varepsilon = \mathrm{La}_{min}/\ \mathrm{La}_{Hinze}$, where La_{Hinze} is the value of La for the Hinze bubble radius, about 2 mm,[17] i.e., $\mathrm{La}_{Hinze} \simeq 1.5\times10^5$.

Alternatively, q can be expressed as a p.d.f. for the stochastic variable La as $q(x) = \langle\ \mathrm{La}\ \rangle\theta(La)$, where the first moment of $\theta(\ \mathrm{La}\ )$ $(s=1)$ is $\langle\ \mathrm{La}\ \rangle$. Regarding the values of d and the exponents a and c, the following considerations apply:

(1) At La = La_{Hinze}, the probability distribution abruptly changes the power-law dependence to a new exponent theoretically equal to $-10/3$.[17] Fitting the power-law to the data, the local shape factor d should be around 3, and the exponent c approximately equals to -4 (close but different from $-10/3$ for $R_o/\langle R_o\rangle \lesssim 40$, see Fig. 11). Interestingly, one has that La_{Hinze} is very close to $\mathrm{La}_{max} \simeq 2\times10^5$, the maximum value of La for which jet droplets are ejected, and therefore, the exponent c plays a secondary role in the global aerosol distribution since film droplets are much smaller than jet droplets in this size range.

(2) The uncertainty of measurements at the Aitken mode range or the sheer absence of data makes a precise determination of the shape of the distribution function and the calculation of the exponent a challenging for $R_o/\langle R_o\rangle < 0.1$, if not useless. This is marked as a dotted line in Fig. 11. Since no droplets are ejected for La $<$ La_{min}, the choice of La_{min} as the turning point where the bubble size distribution decays, at least from the droplet generation side, is consistent. The calculations for the global aerosol distribution are insensitive to a values as long as the decay exponent a is steeper than 3 for $R_o/\langle R_o\rangle \to 0$.

An important question raised by Néel and Deike[41] is whether the actual probability distribution of bubbles popping at the surface of seawater is reproduced by the probability distribution measured in the bulk, given by (9). While a one-to-one correspondence was assumed in Berny *et al.*[35] and in Jiang *et al.*,[15] given the very different raising velocities of the bubble size spectrum and the stages of development of the breaking wave, that assumption is called into question. However, it can be sustained as the most statistically consistent one for the purposes of this study since the global ensemble distribution of ejected droplet radii must consider the presence of bubbles, transient cavities, liquid ligaments, films, and spumes necessarily making liquid–gas surfaces present at all scales in the turbulent motion, from about $R_o \sim l_\mu$ to about several centimeters (i.e., more than six orders of magnitude). Thus, bulk bubbles capable of generating jet droplets are actually exposed to liquid surfaces in a turbulent ocean much more frequently than the tranquil raising of bubbles in a laboratory tank.

E. Ensemble droplet size statistics

Once the droplet size statistics, the number of ejected droplets per bursting for each droplet generation mechanism, and the statistics of bubbles are quantitatively described, one can easily calculate the theoretical ensemble probability $P(\chi_d)$ of a given ejected droplet size $\chi_d = r_d/l_\mu$.

The non-dimensional ensemble probability can be understood as the expectancy of the number of droplets n_d as a function of La $= R_o/\mu$ under the combined probability of the variable La (the non-dimensional bubble radius) given by $\theta(\ \mathrm{La}\ )$ and the probability of χ_d for the average droplet radius $\langle\chi_d\rangle = \langle r_d\rangle/l_\mu$, which is a function of La as well,[26,35]

$$P(\chi_d) = \int_0^\infty \theta(\mathrm{La})\frac{p(r_d/\langle r_d\rangle)}{\langle r_d\rangle/l_\mu}\,n_d\,d\mathrm{La} = \int_0^\infty \theta(\mathrm{La})\frac{p(\chi_d/\langle\chi_d\rangle)}{\langle\chi_d\rangle}\,n_d\,d\mathrm{La}, \tag{11}$$

where $p(y=\chi_d/\langle\chi_d\rangle)$ is the Gamma distribution and $\theta(\ \mathrm{La}\ )$ is the p.d.f. of the bubble radius in the liquid bulk beneath the average position of the turbulent liquid free surface. The global average jet droplet radius $\langle\langle\chi_d\rangle\rangle = \langle\langle r_d\rangle\rangle/l_\mu$ is simply

$$\langle\langle \chi_d \rangle\rangle = \int_0^\infty \chi_d P(\chi_d) d\chi_d. \tag{12}$$

The average $\langle \chi_d \rangle$ of the stochastic variable χ_d in a single bursting event is a function of La and Mo only, given by the same expression (2) as that for the value of χ_d for the first ejected droplet (i.e., R/l_μ), but with α_1 as a free parameter depending on the environment. This free parameter should be universal for seawater in air at average ocean atmospheric conditions (pressure and temperature).

Observe that the integration of (11) is performed on the complete La domain, and the kernel vanishes at both La $\to 0$ and ∞. In contrast, the kernel of the aggregated distribution in Berny *et al.*[35] diverges for La $\to 0$: the shape of the aggregated distribution is, therefore, strongly determined by the limits of integration in that work.

III. RESULTS AND DISCUSSION

An inventory of well established datasets of the aerosol concentration spectra from the extensive literature reporting atmospheric aerosol measurements from the ocean is selected, including ultrafine particles in the Aitken and accumulation modes,[29] CCN, and INP. Selection of measurements is made at or around the marine boundary layer (MBL), approximately at the average ocean temperature (15 °C), or in laboratory measurements where the described conditions reasonably reproduce the open ocean ones.[12,17,19,61,72–75] Also, for completeness, the numerical simulation data from Berny *et al.*[35] for bubble swarms are included. Given the width of the aerosol size range (about five orders of magnitude), the ranges of validity of the measurement instruments, the physical effects influencing their performance or the aerosol concentrations measured, and the treatment of samples should be appropriately addressed to build a reasonable overall experimental p.d.f. Obviously, the number concentrations provided by published measurements should be scaled to obtain probability measures. In effect, the collected experimental data from the literature[1,12,16–20,35,61,62,72,75–79] are scaled according to the procedures described in Appendix B to build an experimental probability density function (pdf) $P(\chi_d = r_d/l_\mu)$. The matching of the experimental pdf shape at the overlapping ranges among the different datasets provides a good measure of reliability.

The calculations include an approximate reconstruction of the spray radii from which the given aerosol sizes originate. Given the focus of this work on CCN and INP, their size range is used as the main overlapping range among the different datasets to re-scale the number concentrations and to establish a reasonably continuous pdf. The upper envelope of the experimental datasets is the reference line reducible to a probability distribution. The result is plotted in Fig. 12. Obviously, the requirement of $P(\chi_d)$ being a probability distribution determines the scaling of the different experimental datasets.

A remarkable overall fitting to the proposed model is achieved for $\alpha_1 = 10^{-3}$, with $\langle\langle r_d \rangle\rangle \simeq 0.4\,\mu$m, corresponding to a nascent SSA of average diameter $\langle\langle D_p \rangle\rangle = 200$ nm. The sensitivity of the model to

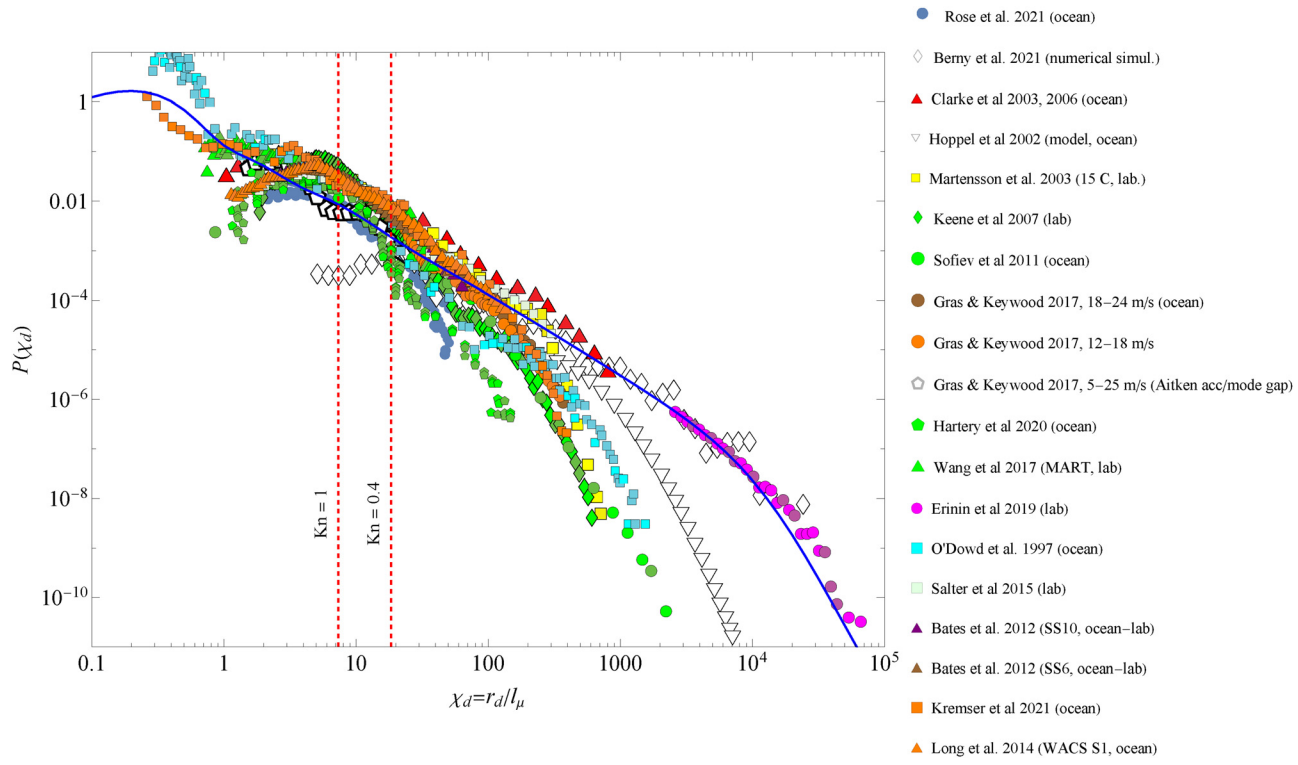

FIG. 12. The probability distribution function $P(\chi_d)$ for the radius $\chi_d = r_d/l_\mu$ of the total ensemble of ejected droplets from the sea at an average temperature of $T = 15^\circ$ C compared to measurements of SSA and OA from different authors. We also note where the measurements were performed for each dataset. The pdf $P(x)$ and the resulting overall average droplet radius $\langle\langle r_d \rangle\rangle \simeq 0.4\,\mu$ m are calculated with $\alpha_1 = 0.001$. The finest aerosol size range described by O'dowd *et al.*[61] could be due to the smallest relics of jet nano-droplets on which VOCs and other vapors condensate.

the main parameter α_1 is given in Appendix C. The result of the model fitting points to an extremely large droplet generation in the nanometric range. This implies the disintegration of extremely thin, nanometric-sized liquid ligaments ejected at enormous speeds (four to five times the average one of air molecules at standard atmospheric conditions) from bursting bubbles from about 5 to 30 μm into several thousands of droplets in the range from about 5 to 20 nm per bubble. This fits reasonably well the extreme ultrafine SSA size spectrum of O'dowd *et al.*[61] for typical maritime North East Atlantic measured number distribution using SMPS. This measured SSA ranged from about 4 to 15 nm would originate from seawater droplets with radii around 0.4–1.2 times the natural length l_μ (19.5 nm for seawater at 15 °C), the size range where the liquid jet acquires its maximum speeds of 4–15 times the natural velocity v_μ (see Ref. 38, p. A12–A17, Fig. 2). To indicate the gas flow regimes, red dashed vertical lines in Fig. 12 indicate the ordinate χ_d values for Kn = 1 and 0.1; between these lines, one has rarefied flow of droplets in the air. At the left of Kn = 1, one has free molecular flow regime.

IV. CONCLUSIONS

The main conclusions and prospectives from this work, on the basis of available evidence, are:

(1) When constructing an ensemble probability density function of the measured oceanic aerosol sizes, film droplet production alone, including the very recently proposed film flapping mechanism,[15] appears to fall orders of magnitude short of explaining the actual numerical concentration of measured aerosols in the sub-micrometer range. First, the energy densities entailed in the liquid film dynamics are insufficient to reach scales comparable or below the natural length scale of seawater, $l_\mu = \mu^2/(\rho\sigma) = 19.5$ nm. Second, the number of droplets produced by the film bursting mechanisms decreases drastically as the bubble radius R_o decreases below 200 μm.
(2) In contrast, not only the bubble size distribution strongly favors bubble sizes between 5 and 200 μm, but also this bubble size range would generate a large number of jet droplets in the sub-micrometer range per bursting event. In effect, the astonishing concentration of kinetic energy per unit volume at the point of collapse for bubble sizes around tens of microns is sufficient to foster jetting at scales much smaller than l_μ.
(3) Microbubbles (specifically, those between 5 and 200 μm) face significant challenges to effectively reach the air–water surface due to low rise speed and dissolution.[80] However, unlike what would occur in bubbling experiments in still (or nearly still) water in a laboratory tank, the actual turbulent sea surface water would be saturated, or even supersaturated with air, from a relatively moderate wind and breaking wave activity. In reality, the turbulent surface of the open sea is a dynamic fractal object whose mean radius of curvature may be below the centimeter or even millimeter scales. This would make always-present millimeter-sized droplets, ligaments, and foams perfect mobile platforms for the bursting of microbubbles, which would increase the volume of water per unit area loaded with those microbubbles exposed to the water–air surface by many orders of magnitude. Although a precise quantification of this mechanism is not yet available and is not the subject of the present work, it would provide a sound basis for the main proposal here made.

These observations would imply a complete reconsideration of the physical pathways of aerosol production from the ocean: the vast majority of these aerosols would have their elusive birth in the uterus-like nano-shape (Fig. 6) of a bursting microbubble in the last instants of collapse. This would have fundamental implications for the understanding of oceanic aerosols and their origin. Naturally, the statistical agreement shown is a necessary but not sufficient condition for an irrefutable attribution to the described mechanisms. However, no other mechanisms with this level of precision have been described so far to explain the origin of sub-micrometer and nanometer scale primary and secondary oceanic aerosols (cloud condensation nuclei, ice particles, volatile organic compound nuclei, and micro- and nanoplastics), and to also explain their high diffusivity from the ocean surface. More importantly, the accuracy of this model is such that it provides an optimal component for ocean aerosol fluxes in global climate models, in the absence of a better solution.

ACKNOWLEDGMENTS

This research was supported by the Spanish Ministry of Economy, Industry and Competitiveness (Grant Nos. DPI2016–78887 and PID2019–108278RB) and by J. de Andalucía (Grant No. P18-FR-3623. Data from numerical simulations made by J. M. López-Herrera, already reported in Ref. 38, are used in this work (Fig. 7), which is especially acknowledged. P. Riesco-Chueca made very useful suggestions. C. de Lorenzo provided insightful comments.

AUTHOR DECLARATIONS

Conflict of Interest

The author has no conflicts to disclose.

Author Contributions

Alfonso M. Gañán-Calvo: Conceptualization (equal); Data curation (equal); Formal analysis (equal); Funding acquisition (equal); Investigation (equal); Methodology (equal); Project administration (equal); Resources (equal); Software (equal); Supervision (equal); Validation (equal); Visualization (equal); Writing – original draft (equal); Writing – review & editing (equal).

DATA AVAILABILITY

The data that support the findings of this study are available from the corresponding author upon reasonable request.

APPENDIX A: EXPERIMENTAL DATA RELIABILITY AND SPECTRAL LIMITS

The spray (primary marine aerosol) size spectra measured in the collection of selected datasets span five orders of magnitude, from ultrafine to coarse particles. This demands the use of measuring instruments based on different technologies: different authors[12,17–19,73,74] have used ultrafine condensation particle counters (e.g., TSI3760,

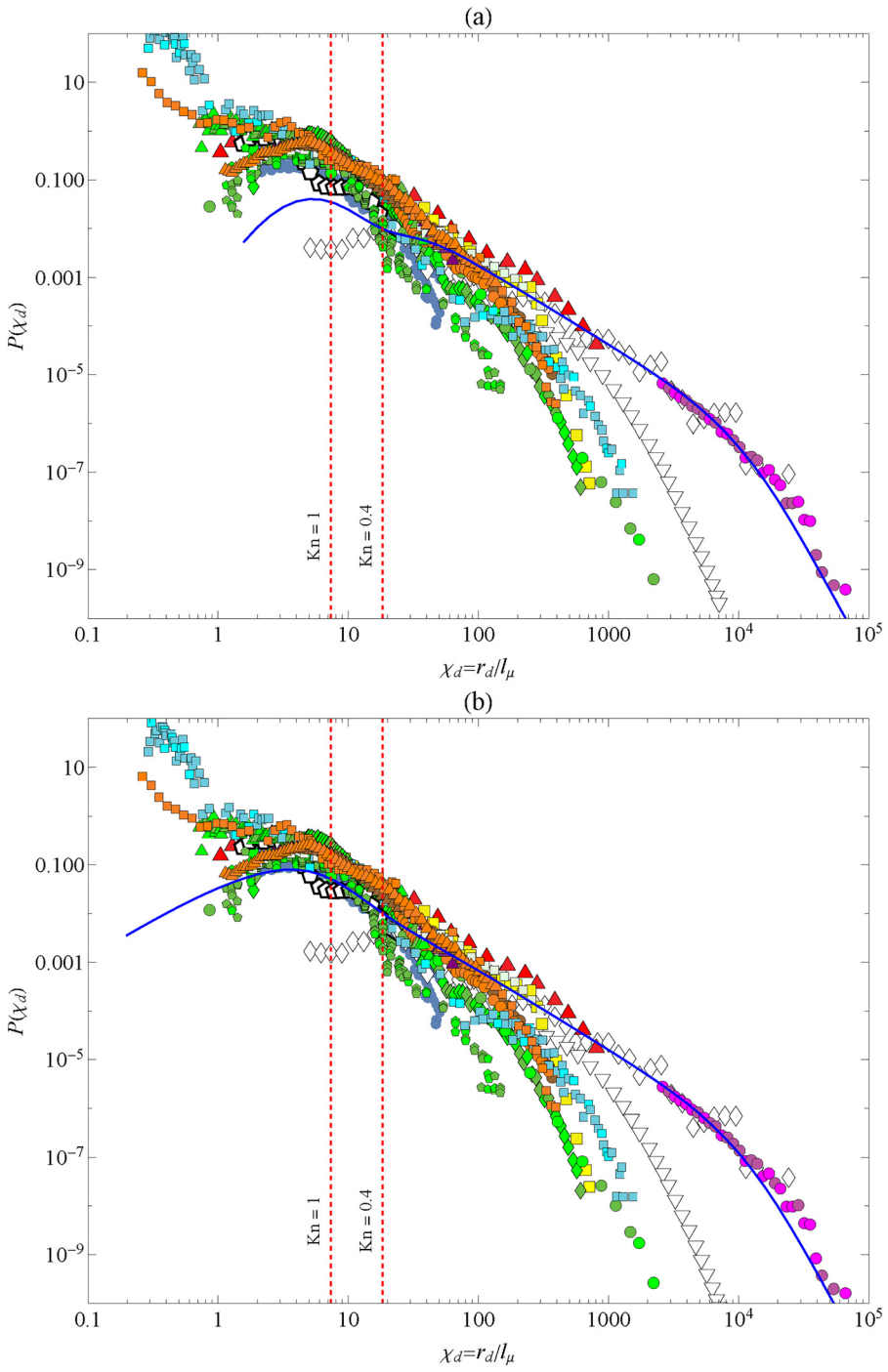

FIG. 13. The probability distribution function $P(\chi_d)$ for the radius $\chi_d = r_d/l_\mu$ of the total ensemble of ejected droplets from the sea at an average temperature of $T = 15^\circ$ C compared to measurements of SSA and OA from different authors. We also note where the measurements were performed for each dataset. The p.d.f. $P(x)$ and the overall average droplet radius $\langle\langle r_d \rangle\rangle$ are calculated with $\alpha_1 =$ (a) 0.133 (see Ref. 38) and (b) 0.02. The corresponding averages $\langle\langle r_d \rangle\rangle$ are 5.3 and 1.3 μm. The ordinate values are automatically adjusted in each plot. Plot markers correspond to those of Fig. 12, main text.

TSI3787, and TSI3010), mobility analyzers (e.g., TSI3081 and TSI3790), aerodynamic particle sizers (e.g., TSI3321), automated static thermal gradient cloud chamber, or active scattering aerosol spectrometer probe (ASASP-X), each of them with a relatively narrow measuring range capability compared to the whole marine spray size span. Consequently, open ocean measurements using these instruments tend to underestimate significantly the actual content of the spray spectra in the air layers in contact with the sea surface, since the size spectrum beyond the accumulation mode tends to settle. The only data correctly representing the actual spray size contents in that region are those from Berny *et al.*,[35] with a direct account—drop by drop—from simulations, and from Erinin *et al.*[75]

APPENDIX B: DATA TREATMENT

The particle size measured under the conditions described in each publication has been carefully converted to droplet radius for each relevant dataset.[1,12,16–20,35,61,62,72,75,77–79,81] Most authors report the values of dry aerosols (obtained with a variety of drying conditions: temperatures from ambient ones, with RH from 80% to 20%, to about 300 °C), except Erinin *et al.*[75] and Berny *et al.*[35] reporting droplet sizes. The remaining humidity in the final state of the measured particle has been considered. The water content of the particle is estimated based on an evaporative model with residues at the corresponding RH of the environment.[82] The converted SSA particle sizes to corresponding droplet radii are scaled with the length scale $l_\mu = 19.5$ nm, measured at the average ocean temperature of 15 °C. In addition, while some authors[35,61,72,75] report the droplet or aerosol radius, the rest give the diameter. The reconstruction of the corresponding droplet size from dry residues is made using a standard 3.5% salt concentration in the ocean.

Either the concentration N per unit volume or the flux spectra reported by the authors, which are strongly dependent on the actual local conditions of measurements (fundamentally wind and wave amplitude[12,16–20]), are scaled to represent a true p.d.f. under the hypothesis that each reported concentration (their ordinates N) correctly describes at least a fraction of the complete number density spectrum. The following procedure is followed:

- The ordinate values N of the distributions disclosed by the different authors are averaged in the interval for Kn $\in \{0.4, 1\}$ (i.e., $r_d \in \{\lambda_a, 2.5\lambda_a\}$), where the most interesting jet droplets features from bubble bursting phenomena begin to occur (rarefied conditions). To do so, an interpolation function $f_i(\chi_d)$ for each dataset is integrated in the interval $\chi_d \in \{\lambda_a/l\mu, 2.5\lambda_a/l_\mu\}$, so that $F_i = \int_{\lambda_a/l\mu}^{2.5\lambda_a/l\mu} f_i(\chi_d)d\chi_d$.
- For a given value of α_1, the ordinate values of each dataset are divided by F_i and multiplied by the averaged value (say P_K) of the theoretical p.d.f. in the interval $\chi_d \in \{\lambda_a/l\mu, 2.5\lambda_a/l_\mu\}$, i.e., $P_K = \int_{\lambda_a/l\mu}^{2.5\lambda_a/l\mu} P(\chi_d)d\chi_d$.
- The resulting scaled values of the experimental distributions are compared to the theoretical distribution in the whole interval (see Figs. 12 and 13). In some cases (e.g., Ref. 75), the experimental interval of r_d values disclosed does not cover the rarefied conditions. In this case, the experimental p.d.f. is scaled to match the theoretical p.d.f. at the center of the interval of interest.

APPENDIX C: MODEL SENSITIVITY TO THE FREE PARAMETER α_1

Figure 13 shows the fitting of the model given by Eq. (11), main text, to the datasets, under different hypotheses:

(1) Figure 13(a): The model uses the fittings constants published in Gañán-Calvo and López-Herrera[38] ($\alpha_1 = 0.133$ and $\mathrm{Oh}_c = 0.03$, or $\mathrm{La}_c = 1111$), obtained from available data on individual BB using several different liquids, which, in the range of Laplace numbers, yield measurable ejections. Naturally, these ejections happen in air at atmospheric conditions, and their characteristic speeds are sufficiently smaller than the speed of sound to assume incompressibility throughout the whole bursting and ejection events. The model perfectly fits the numerical simulation data from Ref. 35, which were made under these hypotheses (see Fig. 5, main text). The contribution of the flapping droplets[15] would be maximum in the range of CCN marked for this value of the free parameter ($\alpha_1 = 0.133$).

(2) Figure 13(b): This intermediate model prediction uses an intermediate fitting ($\alpha_1 = 0.02$) between those which fits the numerical simulations of Berny *et al.*[37] ($\alpha_1 = 0.032$) and from Gañán-Calvo and López-Herrera[38] ($\alpha_1 = 0.003$), see Fig. 5, main text. With some caveats, $\alpha_1 = 0.02$ would fit nearly all datasets, except the extreme ultrafine spectrum measured by O'Dowd *et al.*[61] The contribution of flapping droplets would completely vanish compared to that of jet droplets for this α_1 value.

The bubbles producing the size range predicted in Fig. 10, main text, should be present in surface seawater fully saturated (or supersaturated) with air. These conditions are, indeed, met under continuous wave breaking:[8,12] due to their large internal air pressure, they should diffuse air into the surrounding water very effectively. In addition, each bursting bubble in the range from 10 to 500 μm can generate tiny bubbles that get trapped at the bottom of the cavity in the liquid,[38,43,83] which increases the air supersaturation at the surface microlayer.

REFERENCES

[1] T. S. Bates, P. K. Quinn, A. A. Frossard, L. M. Russell, J. Hakala, T. Petäjä, M. Kulmala, D. S. Covert, C. D. Cappa, S. M. Li, K. L. Hayden, I. Nuaaman, R. McLaren, P. Massoli, M. R. Canagaratna, T. B. Onasch, D. Sueper, D. R. Worsnop, and W. C. Keene, "Measurements of ocean derived aerosol off the coast of California," J. Geophys. Res.: Atmos. **117**, 1–13, https://doi.org/10.1029/2012JD017588 (2012).

[2] P. Schmitt-Kopplin, G. Liger-Belair, B. P. Koch, R. Flerus, G. Kattner, M. Harir, B. Kanawati, M. Lucio, D. Tziotis, N. Hertkorn, and I. Gebefügi, "Dissolved organic matter in sea spray: A transfer study from marine surface water to aerosols," Biogeosciences **9**, 1571–1582 (2012).

[3] T. H. Bertram, R. E. Cochran, V. H. Grassian, and E. A. Stone, "Sea spray aerosol chemical composition: Elemental and molecular mimics for laboratory studies of heterogeneous and multiphase reactions," Chem. Soc. Rev. **47**, 2374–2400 (2018).

[4] S. D. Brooks and D. C. O. Thornton, "Marine aerosols and clouds," Annu. Rev. Mar. Sci. **10**, 289–313 (2018).

[5] J. V. Trueblood, X. Wang, V. W. Or, M. R. Alves, M. V. Santander, K. A. Prather, and V. H. Grassian, "The old and the new: Aging of sea spray aerosol and formation of secondary marine aerosol through OH oxidation reactions," ACS Earth Space Chem. **3**, 2307–2314 (2019).

[6] K. J. Mayer, X. Wang, M. V. Santander, B. A. Mitts, J. S. Sauer, C. M. Sultana, C. D. Cappa, and K. A. Prather, "Secondary marine aerosol plays a dominant role over primary sea spray aerosol in cloud formation," ACS Cent. Sci. **6**, 2259–2266 (2020).

[7] B. A. Mitts, X. Wang, D. D. Lucero, C. M. Beall, G. B. Deane, P. J. DeMott, and K. A. Prather, "Importance of supermicron ice nucleating particles in nascent sea spray," Geophys. Res. Lett. **48**, 1–10, https://doi.org/10.1029/2020GL089633 (2021).

[8] L. Deike, "Mass transfer at the ocean-atmosphere interface: The role of wave breaking, droplets, and bubbles," Annu. Rev. Fluid Mech. **54**, 191–224 (2022).

[9] K. J. Angle, D. R. Crocker, R. M. C. Simpson, K. J. Mayer, L. A. Garofalo, A. N. Moore, S. L. M. Garcia, V. W. Or, S. Srinivasan, M. Farhan, J. S. Sauer, C. Lee, M. A. Pothier, D. K. Farmer, T. R. Martz, T. H. Bertram, C. D. Cappa, K. A. Prather, and V. H. Grassian, "Acidity across the interface from the ocean surface to sea spray aerosol," Proc. Natl. Acad. Sci. U.S.A. **118**, e2018397118 (2021).

[10]G. C. Cornwell, C. S. McCluskey, P. J. DeMott, K. A. Prather, and S. M. Burrows, "Development of heterogeneous ice nucleation rate coefficient parameterizations from ambient measurements," Geophys. Res. Lett. **48**, e2021GL095359, https://doi.org/10.1029/2021GL095359 (2021).
[11]R. E. Cochran, O. S. Ryder, V. H. Grassian, and K. A. Prather, "Sea spray aerosol: The chemical link between the oceans, atmosphere, and climate," Acc. Chem. Res. **50**, 599–604 (2017).
[12]X. Wang, G. B. Deane, K. A. Moore, O. S. Ryder, M. D. Stokes, C. M. Beall, D. B. Collins, M. V. Santander, S. M. Burrows, C. M. Sultana, and K. A. Prather, "The role of jet and film drops in controlling the mixing state of submicron sea spray aerosol particles," Proc. Natl. Acad. Sci. U.S.A. **114**, 6978–6983 (2017).
[13]L. Liu, L. Du, L. Xu, J. Li, and N. T. Tsona, "Molecular size of surfactants affects their degree of enrichment in the sea spray aerosol formation," Environ. Res. **206**, 112555 (2022).
[14]R. Penrose, *The Large, the Small and the Human Mind* (Cambridge University Press, New York, NY, 2000).
[15]X. Jiang, L. Rotily, E. Villermaux, and X. Wang, "Submicron drops from flapping bursting bubbles," Proc. Natl. Acad. Sci. U.S.A. **119**, e2112924119 (2022).
[16]G. B. Deane and M. D. Stokes, "Scale dependence of bubble creation mechanisms in breaking waves," Nature **418**, 839–844 (2002).
[17]A. D. Clarke, V. Kapustin, S. Howell, K. Moore, S. Masonis, T. Anderson, and D. Covert, "Sea-salt size distributions from breaking waves: Implications for marine aerosol production and optical extinction measurements during seas," J. Atmos. Oceanic Technol. **20**, 1362–1374 (2003).
[18]A. D. Clarke, S. R. Owens, and J. Zhou, "An ultrafine sea-salt flux from breaking waves: Implications for cloud condensation nuclei in the remote marine atmosphere," J. Geophys. Res.: Atmos. **111**, D06202, https://doi.org/10.1029/2005JD006565 (2006).
[19]M. Sofiev, J. Soares, M. Prank, G. D. Leeuw, and J. Kukkonen, "A regional-to-global model of emission and transport of sea salt particles in the atmosphere," J. Geophys. Res.: Atmos. **116**, D21302, https://doi.org/10.1029/2010JD014713 (2011).
[20]P. K. Quinn, D. B. Collins, V. H. Grassian, K. A. Prather, and T. S. Bates, "Chemistry and related properties of freshly emitted sea spray aerosol," Chem. Rev. **115**, 4383–4399 (2015).
[21]A. H. Woodcock, C. F. Kientzler, A. B. Arons, and D. C. Blanchard, "Giant condensation nuclei from bursting bubbles," Nature **172**, 1144–1145 (1953).
[22]R. J. Cipriano and D. C. Blanchard, "Bubble and aerosol spectra produced by a laboratory 'breaking wave,'" J. Geophys. Res. **86**, 8085, https://doi.org/10.1029/JC086iC09p08085 (1981).
[23]D. C. Blanchard and L. D. Syzdek, "Film drop production as a function of bubble size," J. Geophys. Res. **93**, 3649–3654, https://doi.org/10.1029/JC093iC04p03649 (1988).
[24]D. E. Spiel, "On the births of jet drops from bubbles bursting on water surfaces," J. Geophys. Res. **100**, 4995–5006, https://doi.org/10.1029/94JC03055 (1995).
[25]E. Lewis and S. Schwartz, "Sea salt aerosol production: Mechanisms, methods, measurements and models—A critical review," Geophys. Monogr. Ser. **152**, 1–408 (2004).
[26]H. Lhuissier and E. Villermaux, "Bursting bubble aerosols," J. Fluid Mech. **696**, 5–44 (2012).
[27]A. M. Worthington, *A Study of Splashes* (Longmans, Green and Co., London, 1908).
[28]S. G. Boyce, "The salt spray community," Ecol. Monogr. **24**, 29–67 (1954).
[29]M. L. Pöhlker, M. Zhang, R. C. Braga, O. O. Krüger, U. Pöschl, and B. Ervens, "Aitken mode particles as CCN in aerosol- and updraft-sensitive regimes of cloud droplet formation," Atmos. Chem. Phys. **21**, 11723–11740 (2021).
[30]F. J. Resch, J. S. Darrozes, and G. M. Afeti, "Marine liquid aerosol production from bursting of air bubbles," J. Geophys. Res. **91**, 1019, https://doi.org/10.1029/JC091iC01p01019 (1986).
[31]J. Wu, "Production functions of film drops by bursting bubbles," J. Phys. Oceanogr. **31**, 3249–3257 (2001).
[32]K. A. Prather, T. H. Bertram, V. H. Grassian, G. B. Deane, M. D. Stokes, P. J. DeMott, L. I. Aluwihare, B. P. Palenik, F. Azam, J. H. Seinfeld, R. C. Moffet, M. J. Molina, C. D. Cappa, F. M. Geiger, G. C. Roberts, L. M. Russell, A. P. Ault, J. Baltrusaitis, D. B. Collins, C. E. Corrigan, L. A. Cuadra-Rodriguez, C. J. Ebben, S. D. Forestieri, T. L. Guasco, S. P. Hersey, M. J. Kim, W. F. Lambert, R. L. Modini, W. Mui, B. E. Pedler, M. J. Ruppel, O. S. Ryder, N. G. Schoepp, R. C. Sullivan, and D. Zhao, "Bringing the ocean into the laboratory to probe the chemical complexity of sea spray aerosol," Proc. Natl. Acad. Sci. U.S.A. **110**, 7550–7555 (2013).
[33]M. Cunliffe, A. Engel, S. Frka, B. Ž. Gašparović, C. Guitart, J. C. Murrell, M. Salter, C. Stolle, R. Upstill-Goddard, and O. Wurl, "Sea surface microlayers: A unified physicochemical and biological perspective of the air-ocean interface," Prog. Oceanogr. **109**, 104–116 (2013).
[34]J. T. Hardy, "The sea surface microlayer: Biology, chemistry and anthropogenic enrichment," Prog. Oceanogr. **11**, 307–328 (1982).
[35]A. Berny, S. Popinet, T. Séon, and L. Deike, "Statistics of jet drop production," Geophys. Res. Lett. **48**, e2021GL092919, https://doi.org/10.1029/2021GL092919 (2021).
[36]C. F. Brasz, C. T. Bartlett, P. L. Walls, E. G. Flynn, Y. E. Yu, and J. C. Bird, "Minimum size for the top jet drop from a bursting bubble," Phys. Rev. Fluids **3**, 074001 (2018).
[37]A. Berny, L. Deike, T. Séon, and S. Popinet, "Role of all jet drops in mass transfer from bursting bubbles," Phys. Rev. Fluids **5**, 033605 (2020).
[38]A. M. Gañán-Calvo and J. M. López-Herrera, "On the physics of transient ejection from bubble bursting," J. Fluid Mech. **929**, A12 (2021).
[39]A. Berny, L. Deike, S. Popinet, and T. Séon, "Size and speed of jet drops are robust to initial perturbations," Phys. Rev. Fluids **7**, 013602 (2022).
[40]H. Lhuissier and E. Villermaux, "Soap films burst like flapping flags," Phys. Rev. Lett. **103**, 054501 (2009).
[41]B. Néel and L. Deike, "Collective bursting of free-surface bubbles, and the role of surface contamination," J. Fluid Mech. **917**, A46 (2021).
[42]Y. Toba, "Drop production by bursting of air bubbles on the sea surface. II. Theoretical study on the shape of floating bubbles," J. Oceanogr. Soc. Jpn. **15**, 121–130 (1959).
[43]L. Duchemin, S. Popinet, C. Josserand, and S. Zaleski, "Jet formation in bubbles bursting at a free surface," Phys. Fluids **14**, 3000–3008 (2002).
[44]D. B. Shaw and L. Deike, "Surface bubble coalescence," J. Fluid Mech. **915**, A105 (2021).
[45]A. M. Gañán-Calvo, "The complexity of aerosol production from bubble bursting," PNAS **219**, e2208770119 (2022).
[46]A. M. Gañán-Calvo, "Revision of bubble bursting: Universal scaling laws of top jet drop size and speed," Phys. Rev. Lett. **119**, 204502 (2017).
[47]P. L. Walls, L. Henaux, and J. C. Bird, "Jet drops from bursting bubbles: How gravity and viscosity couple to inhibit droplet production," Phys. Rev. E **92**, 021002(R) (2015).
[48]E. Ghabache and T. Séon, "Size of the top jet drop produced by bubble bursting," Phys. Rev. Fluids **1**, 051901 (2016).
[49]J. S. Lee, B. M. Weon, S. J. Park, J. H. Je, K. Fezzaa, and W. K. Lee, "Size limits the formation of liquid jets during bubble bursting," Nat. Commun. **2**, 367 (2011).
[50]F. Garner, S. Ellis, and J. Lacey, "The size distribution and entrainment of droplets," Trans. Inst. Chem. Eng. **32**, 222–235 (1954).
[51]S. Hayami and Y. Toba, "Drop production by bursting of air bubbles on the sea surface. I. Experiments at still sea water surface," J. Oceanogr. Soc. Jpn. **14**, 145 (1958).
[52]R. Tedesco and D. Blanchard, "The size distribution and entrainment of droplets," J. Rech. Atmos. **13**, 215–226 (1954).
[53]D. C. Blanchard, "The size and height to which jet drops are ejected from bursting bubbles in seawater," J. Geophys. Res. **94**, 10999, https://doi.org/10.1029/JC094iC08p10999 (1989).
[54]M. Sakai, "Ion distribution at a nonequilibrium gas/liquid interface," J. Colloid Interface Sci **127**, 156–166 (1989).
[55]T. Séon and G. Liger-Belair, "Effervescence in champagne and sparkling wines: From bubble bursting to droplet evaporation," Eur. Phys. J.: Spec. **226**, 117–156 (2017).
[56]S. Popinet, see http://basilisk.fr/ for "Basilisk flow solver and PDE library, 2015;" accessed 24 February 2021.
[57]M. Moseler and U. Landman, "Formation, stability, and breakup of nanojets," Science **289**, 1165–1169 (2000).
[58]J. M. Montanero and A. M. Gañán-Calvo, "Jetting, dripping and tip streaming," Rep. Prog. Phys. **83**, 097001 (2020).

[59]J. Rosell-Llompart and J. F. de la Mora, "Generation of monodisperse droplets 0.3 to 4 micrometre in diameter from electrified cone-jets of highly conducting and viscous liquids," J. Aerosol Sci. **25**, 1093–1119 (1994).
[60]E. Villermaux, P. Marmottant, and J. Duplat, "Ligament-mediated spray formation," Phys. Rev. Lett. **92**, 074501 (2004).
[61]C. D. O'dowd, M. H. Smith, I. E. Consterdine, and J. A. Lowe, "Marine aerosol, sea-salt, and the marine sulphur cycle: A short review," Atmos. Environ. **31**, 73–80 (1997).
[62]S. Kremser, M. Harvey, P. Kuma, S. Hartery, A. Saint-Macary, J. McGregor, A. Schuddeboom, M. Von Hobe, S. T. Lennartz, A. Geddes, R. Querel, A. McDonald, M. Peltola, K. Sellegri, I. Silber, C. S. Law, C. J. Flynn, A. Marriner, T. C. Hill, P. J. Demott, C. C. Hume, G. Plank, G. Graham, and S. Parsons, "Southern Ocean cloud and aerosol data: A compilation of measurements from the 2018 southern ocean ross sea marine ecosystems and environment voyage," Earth Syst. Sci. Data **13**, 3115–3153 (2021).
[63]P. H. Dahl and A. T. Jessup, "On bubble clouds produced by breaking waves: An event analysis of ocean acoustic measurements," J. Geophys. Res. **100**, 5007–5020, https://doi.org/10.1029/94JC03019 (1995).
[64]G. B. Deane and M. D. Stokes, "Model calculations of the underwater noise of breaking waves and comparison with experiment," J. Acoust. Soc. Am. **127**, 3394–3410 (2010).
[65]A. M. Gañán-Calvo, "Scaling laws of top jet drop size and speed from bubble bursting including gravity and inviscid limit," Phys. Rev. Fluids **3**, 091601(R) (2018).
[66]J. Eggers, M. A. Fontelos, D. Leppinen, and J. H. Snoeijer, "Theory of the collapsing axisymmetric cavity," Phys. Rev. Lett. **98**, 094502 (2007).
[67]L. Deike, E. Ghabache, G. Liger-Belair, A. K. Das, S. Zaleski, S. Popinet, and T. Séon, "Dynamics of jets produced by bursting bubbles," Phys. Rev. Fluids **3**, 013603 (2018).
[68]S. Chandrasekhar, *Hydrodynamic and Hydromagnetic Stability* (Dover, New York, 1961).
[69]C. Zhao, D. A. Lockerby, and J. E. Sprittles, "Dynamics of liquid nanothreads: Fluctuation-driven instability and rupture," Phys. Rev. Fluids **5**, 044201 (2020).
[70]C. E. Blenkinsopp and J. R. Chaplin, "Bubble size measurements in breaking waves using optical fiber phase detection probes," IEEE J. Ocean. Eng. **35**, 388–401 (2010).
[71]R. S. Al-Lashi, S. R. Gunn, E. G. Webb, and H. Czerski, "A novel high-resolution optical instrument for imaging oceanic bubbles," IEEE J. Oceanic Eng. **43**, 72–82 (2018).
[72]W. A. Hoppel, G. M. Frick, and J. W. Fitzgerald, "Surface source function for sea-salt aerosol and aerosol dry deposition to the ocean surface," J. Geophys. Res.: Atmos. **107**, 7–17, https://doi.org/10.1029/2001JD002014 (2002).
[73]E. M. Martensson, E. D. Nilsson, G. de Leeuw, L. H. Cohen, and H. C. Hansson, "Laboratory simulations and parameterization of the primary marine aerosol production," J. Geophys. Res.: Atmos. **108**, 4297, https://doi.org/10.1029/2002JD002263 (2003).
[74]L. J. Gras and M. Keywood, "Cloud condensation nuclei over the southern ocean: Wind dependence and seasonal cycles," Atmos. Chem. Phys. **17**, 4419–4432 (2017).
[75]M. A. Erinin, S. D. Wang, R. Liu, D. Towle, X. Liu, and J. H. Duncan, "Spray generation by a plunging breaker," Geophys. Res. Lett. **46**, 8244–8251, https://doi.org/10.1029/2019GL082831 (2019).
[76]M. Long, W. Keene, D. Kieber, A. Frossard, L. Russell, J. Maben, J. Kinsey, P. Quinn, and T. Bates, "Light-enhanced primary marine aerosol production from biologically productive seawater," Geophys. Res. Lett. **41**, 2661–2670, https://doi.org/10.1002/2014GL059436 (2014).
[77]M. E. Salter, P. Zieger, J. C. A. Navarro, H. Grythe, A. Kirkeväg, B. Rosati, I. Riipinen, and E. D. Nilsson, "An empirically derived inorganic sea spray source function incorporating sea surface temperature," Atmos. Chem. Phys. **15**, 11047–11066 (2015).
[78]S. Hartery, D. Toohey, L. Revell, K. Sellegri, P. Kuma, M. Harvey, and A. J. McDonald, "Constraining the surface flux of sea spray particles from the southern ocean," J. Geophys. Res. Atmos. **125**, e2019JD032026, https://doi.org/10.1029/2019JD032026 (2020).
[79]C. Rose, M. Collaud Coen, E. Andrews, Y. Lin, I. Bossert, C. Lund Myhre, T. Tuch, A. Wiedensohler, M. Fiebig, P. Aalto, A. Alastuey, E. Alonso-Blanco, M. Andrade, B. Artinano, T. Arsov, U. Baltensperger, S. Bastian, O. Bath, J. P. Beukes, B. T. Brem, N. Bukowiecki, J. A. Casquero-Vera, S. Conil, K. Eleftheriadis, O. Favez, H. Flentje, M. I. Gini, F. J. Gomez-Moreno, M. Gysel-Beer, A. G. Hallar, I. Kalapov, N. Kalivitis, A. Kasper-Giebl, M. Keywood, J. E. Kim, S. W. Kim, A. Kristensson, M. Kulmala, H. Lihavainen, N. H. Lin, H. Lyamani, A. Marinoni, S. Martins Dos Santos, O. L. Mayol-Bracero, F. Meinhardt, M. Merkel, J. M. Metzger, N. Mihalopoulos, J. Ondracek, M. Pandolfi, N. Perez, T. Petaja, J. E. Petit, D. Picard, J. M. Pichon, V. Pont, J. P. Putaud, F. Reisen, K. Sellegri, S. Sharma, G. Schauer, P. Sheridan, J. P. Sherman, A. Schwerin, R. Sohmer, M. Sorribas, J. Sun, P. Tulet, V. Vakkari, P. G. Van Zyl, F. Velarde, P. Villani, S. Vratolis, Z. Wagner, S. H. Wang, K. Weinhold, R. Weller, M. Yela, V. Zdimal, and P. Laj, "Seasonality of the particle number concentration and size distribution: A global analysis retrieved from the network of global atmosphere watch (GAW) near-surface observatories," Atmos. Chem. Phys. **21**, 17185–17223 (2021).
[80]S. Thorpe, P. Bowyer, and D. Woolf, "Some factors affecting the size distributions of oceanic bubbles," J. Phys. Oceanogr. **22**, 382–389 (1992).
[81]A. A. Frossard, V. Gérard, P. Duplessis, J. D. Kinsey, X. Lu, Y. Zhu, J. Bisgrove, J. R. Maben, M. S. Long, R. Y. Chang, S. R. Beaupré, D. J. Kieber, W. C. Keene, B. Nozière, and R. C. Cohen, "Properties of seawater surfactants associated with primary marine aerosol particles produced by bursting bubbles at a model air-sea interface," Environ. Sci. Technol. **53**, 9407–9417 (2019).
[82]R. Holyst, M. Litniewski, D. Jakubczyk, K. Kolwas, M. Kolwas, K. Kowalski, S. Migacz, S. Palesa, and M. Zientara, "Evaporation of freely suspended single droplets: Experimental, theoretical and computational simulations," Rep. Prog. Phys. **76**, 034601 (2013).
[83]S. Krishnan, E. J. Hopfinger, and B. A. Puthenveettil, "On the scaling of jetting from bubble collapse at a liquid surface," J. Fluid Mech. **822**, 791–812 (2017).